

Spatial distribution and consequences of contaminants in harbour sediments : A case study from Richards Bay Harbour, South Africa

Mehlhorn, P., Viehberg, F., Kirsten, K., Newman, B., Frenzel, P., Gildeeva, O., Green, A., Hahn, A. & Haberzettl, T.

Published PDF deposited in Coventry University's Repository

Original citation:

Mehlhorn, P, Viehberg, F, Kirsten, K, Newman, B, Frenzel, P, Gildeeva, O, Green, A, Hahn, A & Haberzettl, T 2021, 'Spatial distribution and consequences of contaminants in harbour sediments : A case study from Richards Bay Harbour, South Africa', *Marine Pollution Bulletin*, vol. 172, 112764.

<https://doi.org/10.1016/j.marpolbul.2021.112764>

DOI 10.1016/j.marpolbul.2021.112764

ISSN 0025-326X

ESSN 1879-3363

Publisher: Elsevier

[Publisher statement]

This is an Open Access article distributed under the terms of the Creative Commons Attribution License (<http://creativecommons.org/licenses/by/4.0/>), which permits unrestricted use, distribution, and reproduction in any medium, provided the original work is properly cited.



Spatial distribution and consequences of contaminants in harbour sediments – A case study from Richards Bay Harbour, South Africa

Paul Mehlhorn^{a,*}, Finn Viehberg^a, Kelly Kirsten^b, Brent Newman^{c,d}, Peter Frenzel^e,
Olga Gildeeva^e, Andrew Green^{f,g}, Annette Hahn^h, Torsten Haberzettl^a

^a University of Greifswald, Institute for Geography and Geology, F.L.-Jahn Str. 16, 17489 Greifswald, Germany

^b University of Cape Town, Department of Geological Sciences, South Lane, Upper Campus, 7701 Rondebosch, South Africa

^c Coastal Systems Research Group, CSIR, P.O. Box 59081, Umbilo, 4075 Durban, South Africa

^d Nelson Mandela University, P.O. Box 77000, Port Elizabeth 6031, South Africa

^e Friedrich-Schiller-University Jena, Institute of Geosciences, Burgweg 11, 07749 Jena, Germany

^f Geological Sciences, University of KwaZulu-Natal, Private Bag X54001, Durban 4000, South Africa

^g School of Geography and Environmental Sciences, Ulster University, Coleraine BT52 1SA, UK

^h University of Bremen, MARUM – Center for Marine Environmental Sciences, Leobener Str. 8, 28359 Bremen, Germany

ARTICLE INFO

Keywords:

Metal contamination
Chromium
Magnetic susceptibility
Microplastics
Calcareous microfossils
Sediment

ABSTRACT

Richards Bay Harbour (RBH) is situated in the industrialized area on the northeast coast of South Africa. To decipher recent human activities and accompanying environmental degradation, surface sediment was collected across RBH and analysed for granulometric and elemental composition, microfaunal assemblages, and microplastics. Microplastics occur most abundantly near recreational areas, whereas metal contamination relates to activities at bulk goods terminals from which they are imported or exported. In particular, Cr and Cu concentrations in surface sediment near bulk goods terminals exceed South African sediment quality guidelines. In metal contaminated sediment, bioindicators reflected stress and were noticeably impacted. A transect of short sediment cores reflects spatial and historical metal contamination and allows quantification of the load of metals within the sediment column. The volume of metal (Cr) contaminated sediment was estimated at almost 2 million m³.

1. Introduction

South Africa's northeast coast is becoming increasingly pressured by human activity. This anthropogenic impact, combined with effects of climate change, places stress on aquatic and terrestrial environments (Department of Environmental Affairs, 2012a). Richards Bay was one of the last remaining undisturbed large estuaries on the KwaZulu-Natal coast (Cloete and Oliff, 1976) until the establishment of Richards Bay Harbour (RBH) in the early 1970s.

The original estuary was a sheltered coastal waterbody open to the ocean (Whitfield, 1992). During harbour construction, the basin's topography and river connection were changed fundamentally, by placing a berm that divided the estuary (Fig. 1). This disconnected today's port from the Mhlatuze River, which now only feeds a natural sanctuary to the south of the berm (Figs. 1, 3). Thus, riverine water, sediment discharge, and agricultural nutrient input from the Mhlatuze

catchment does not reach the harbour (Cloete and Oliff, 1976). Since construction, RBH has been under full marine influence apart from minor freshwater inflows via the Mzingazi and Bhizolo Canals (Begg, 1978). The Mzingazi Canal connects to Lake Mzingazi, which is a subordinate freshwater supply (Fig. 1).

RBH is a deep water port (permissible draught of 17.5–19.5 m) that was constructed to facilitate the export of coal, but also to serve the needs of two aluminium smelters, a granular fertilizer and sulphuric and phosphoric acid plant, and the export of heavy minerals mined nearby (Goodenough, 2003; Schwab and Becker, 2014). Additional industry, including wood chip processing and a ferrochrome smelter, has since established in the area. The contemporary industrial sector of the region makes RBH susceptible to pollution. The simultaneous accelerated growth of the city of Richards Bay increased its population density and proximity, and increased the threat of contemporary microplastic pollution as well.

* Corresponding author.

E-mail address: paul.mehlhorn@uni-greifswald.de (P. Mehlhorn).

<https://doi.org/10.1016/j.marpolbul.2021.112764>

Received 26 February 2021; Received in revised form 20 July 2021; Accepted 21 July 2021

Available online 20 August 2021

0025-326X/© 2021 The Authors. Published by Elsevier Ltd. This is an open access article under the CC BY license (<http://creativecommons.org/licenses/by/4.0/>).

During the late 1990s, Vermeulen and Wepener (1999) pointed out data gaps in monitoring in RBH since construction of the port. Their subsequent studies analysed metal concentrations in surface sediments of RBH, revealing elevated concentrations of Cr, Cu and Zn in two sub basins (Wepener and Vermeulen, 2005). However, apart from periodic subsequent studies (e.g. Greenfield et al., 2011; Wepener and Degger, 2020), there is little published information on the pollution status of RBH.

The objective of this study was thus to investigate sediment dynamics and the spatial and temporal variation of various pollutants in sediment in RBH, with a focus on metal concentrations and microplastics and the impact of sedimentary metals on diatom, ostracod and foraminifer diversity. The study also makes use of short sediment cores to identify temporal changes in pollution.

2. Materials and methods

2.1. Field methods

In August/September 2018, 86 surface-sediment samples were collected using an Ekman-Birge bottom sampler (HYDROBIOS, Kiel, Germany). The topmost 1 cm of sediment was removed from the grab using a plastic spoon for metal analysis and a metal spoon for organic and microplastic analysis. Aliquots of sediment were transferred to 15 ml Nasco Whirl-Pak's and glass vials (microplastic analyses) and cooled until further processing.

Thirty sediment cores were retrieved using a UWITEC gravity corer (UWITEC, Mondsee, Austria) with 90 mm tube diameter (Fig. 2). The cores were stored at 4 °C in the laboratory until further processing.

During fieldwork, an echo sounder (Garmin echoMap CHIRP 42cv) constantly recorded water depth. These measurements were tide corrected via a tide table provided by the South African Navy Hydrographic Office (SANHO) (high and low stand phases interpolated by local regression). Practical salinity (electrical conductivity) and oxygen were measured using a WTW340i multiprobe (Xylem Inc., Rye Brook, NY, USA).

Multibeam bathymetric data were collected using a Norbit iWBMS 400 kHz narrow beam multibeam echosounder with an integrated inertial navigation system (Applanix WaveMaster II). Sound velocity variation in the water column was inspected using a Valeport sound velocity probe. Positioning and further vessel motion (including tidal variation) were modelled using a Real Time Kinematic GPS. Data were processed in BEAMWORX, where sound velocity casts and tidal

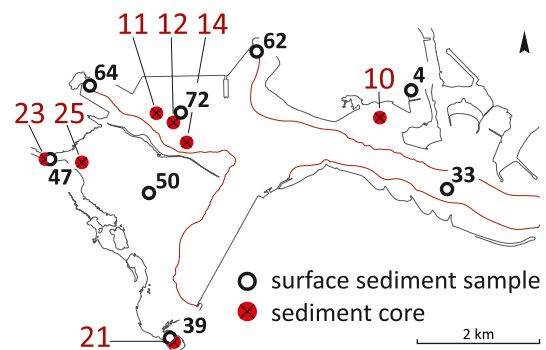


Fig. 2. Sediment short core locations (red dots) and micropaleontology samples (black circles).

variations were integrated into the soundings, spurious soundings were removed, and the final seafloor elevation data was exported as a 0.5 × 0.5 m grid for this study. The data resolved to approximately 10 cm in the vertical domain.

2.2. Grain-size analysis and end member modelling

Aliquots of 0.5–2 g wet sediment were taken for grain-size analyses. The material was soaked in 2 ml hydrochloric acid (HCl, 10%) and 5 ml hydrogen peroxide (H₂O₂, 10%). Residues were dispersed overnight with 5 ml tetrasodium pyrophosphate (Na₄P₂O₇ 10 H₂O, 0.1 M) in an overhead shaker. Subsequently, samples were measured in several runs

Table 1

Information for cores collected in Richards Bay Harbour. Refer to Fig. 2 for core locations.

Core ID locality – year – core number	Recovery date	Latitude [°]	Longitude [°]	Water depth [m]	Core length [cm]
RBH18-10	25 Aug. 18	-28.7976	32.0739	1.6	27.5
RBH18-11	26 Aug. 18	-28.7968	32.0392	20.5	80.5
RBH18-12	26 Aug. 18	-28.7980	32.0419	20.9	118.5
RBH18-14	26 Aug. 18	-28.8007	32.0439	21.0	135.0
RBH18-21	27 Aug. 18	-28.8284	32.0414	4.5	160.0
RBH18-23	27 Aug. 18	-28.8029	32.0220	3.2	72.5
RBH18-25	27 Aug. 18	-28.8034	32.0276	3.5	57.5

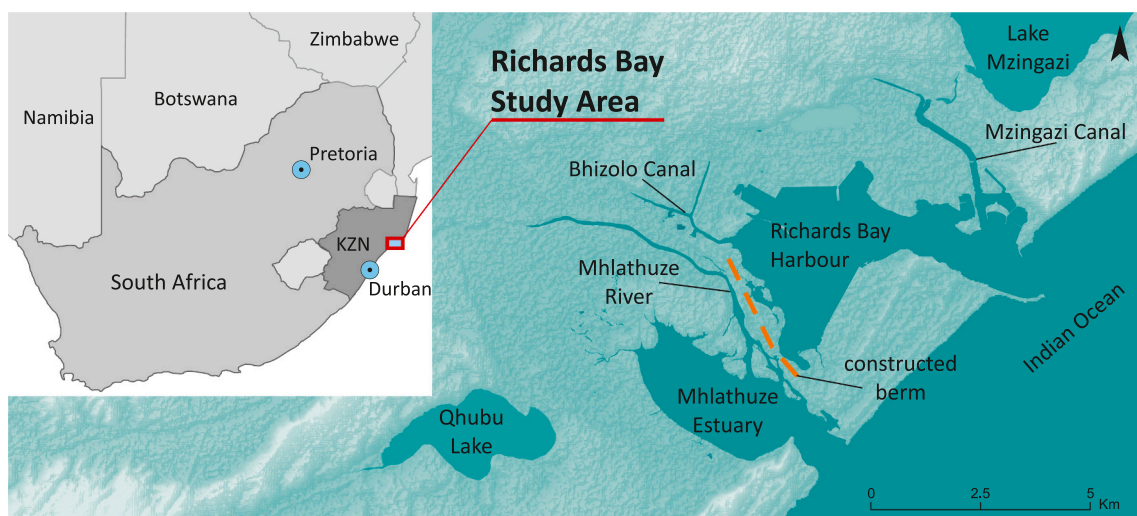


Fig. 1. Richards Bay in continental (left) and regional (right) context. The main river and adjacent lakes are indicated. Highlighted in orange is the berm constructed during the 1970s, which separates Richards Bay Harbour from the Richards Bay Sanctuary (Mhlathuze Estuary).

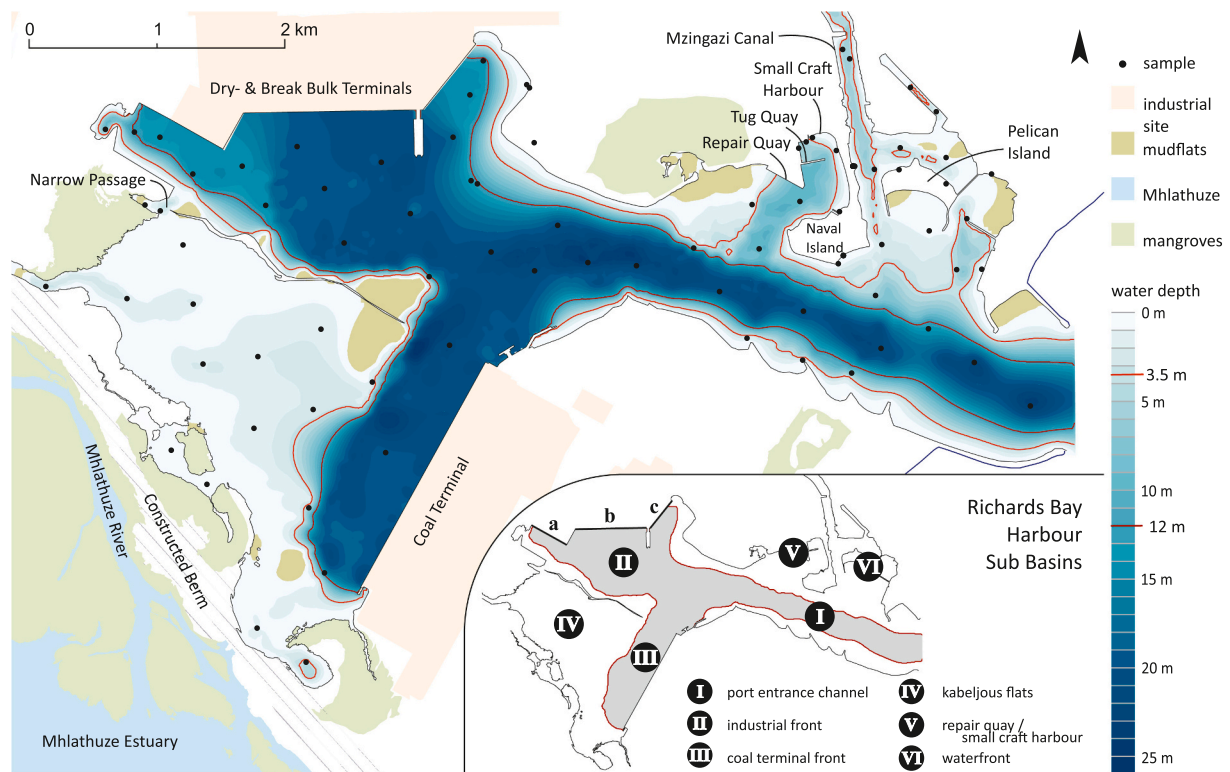


Fig. 3. Bathymetric map of Richards Bay Harbour (tide normalized). Indicated are surface sampling points (black symbols) and landmarks. Dredging results in a steep gradient within the basin marked by steep slope angles indicated by the proximity of the 3.5 and 12 m water depth contour lines. Also indicated are the six sub basins.

using a Laser Diffraction Particle Size Analyser (Fritsch Analysette 22; FRITTSCH GmbH, Germany) until a reproducible signal was obtained. GRADISTAT 8.0 (Blott and Pye, 2001) was used to calculate grain-size statistics. End-member (EM) modelling was carried out using the R software package EMMageo v. 0.9.6. (Dietze and Dietze, 2019).

2.3. Sediment properties and geochemical analyses

Magnetic susceptibility was measured on freeze-dried samples, using a Bartington MS2B sensor and 10 ml plastic cups. For geochemical analyses, freeze-dried samples were ground to a particle size <60 μm and homogenized. Subsamples were digested using a modified aqua regia treatment (100 mg sample, 1.25 ml HCl 37% suprapur and 1.25 ml HNO_3 65% suprapur) in PTFE crucible pressure bombs at 160 $^\circ\text{C}$ for 3 h. Quantitative element concentrations were measured using an Agilent 725 ES ICP-OES (Al, Ca, Fe, K, Mg, Mn, Na, P, S, Sr, Ti) and a Thermo Fischer Scientific X-Series II ICP-MS (As, Cd, Co, Cr, Cu, Ni, Pb, Zn, Rb, Hg). Each digestion batch included laboratory blanks. Calibration was performed with multi element calibration standards. ICP measurements were evaluated using internal standards (20 $\mu\text{g l}^{-1}$ Ru and 10 $\mu\text{g l}^{-1}$ Re). During analysis, calibration verification standards were used regularly, and calibration curves evaluated. Each sample was measured three times, analysed for outliers (Grubbs's test), and reported as the mean and absolute standard deviation.

The Council for Scientific and Industrial Research (CSIR) analysed metal concentrations in 96 surface sediment samples collected in RBH using a van Veen grab in 2012. These data are included in this study for comparative purposes. About 1 g of freeze dried and ball milled sediment was weighed into a digestion vessel and digested in a mixture of HNO_3 -HCl- H_2O_2 according to USEPA method 3050B. The concentrations of metals were measured using a Thermo ICap 6500 ICP-OES (Al, Fe, As, Cu, Cr, Co, Mn, Ni, Pb, Zn) and Agilent 7900 ICP-MS (Cd).

Precision and extraction efficiency of the digestion and metal determination procedures was evaluated by repeatedly analysing marine sediment reference standard PACS-2 (National Research Council of Canada) and sample duplicates.

To properly interpret metal concentrations in sediment the factors that control their natural variation must be compensated for before background or baseline concentrations can be distinguished from enriched (higher than 'expected') concentrations. This is usually accomplished by the procedure of geochemical normalization, wherein metal concentrations are normalized to an element that provides a tracer of crustal decomposition (Hanson et al., 1993; Kerste and Smedes, 2002). In this manner, metal concentrations that are atypical of the bulk of the data can be identified.

Enrichment Factors (EF's) were used to compare metal enrichment of sediment sampled in RBH in 2012 and 2018. Baseline metal concentration models were defined for this purpose, using Al as the normalizer. The models were defined separately for each study since there were (usually small) differences in the nature of relationships between metal and Al concentrations. The differences likely reflect method related differences by the two laboratories that analysed the sediment. The baseline models were defined by fitting a linear regression and 99% prediction limits to scatter plots of metal versus Al concentrations. Metal concentrations falling outside the prediction limits were deemed outliers and sequentially trimmed, starting with the concentration presenting the largest residual and proceeding in this manner until all concentrations fell within the prediction limits. EF's were then computed as the ratio between measured metal concentrations and the concentration at the upper prediction limit at the corresponding Al concentration in the samples. EF's values >1 represent metal concentrations that are higher than expected (Newman and Watling, 2007).

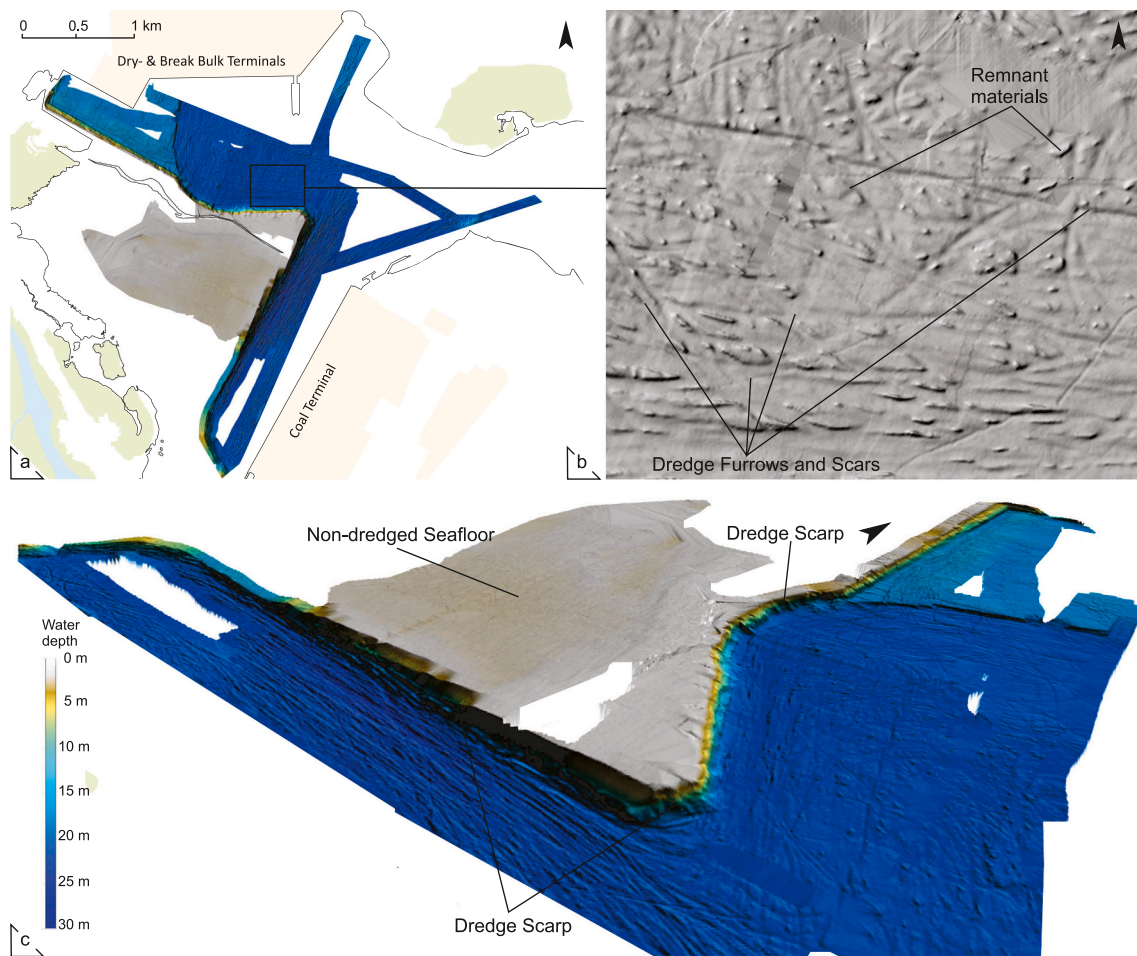


Fig. 4. a) Multibeam echosounder image of SB-I to IV. b) Furrows in sediment surface were created by dredging operations - note the remnants of the pre-dredged material outcrops. c) Steep scarps and sharp edges at the boundary between dredged and un-dredged areas.

2.4. Microplastic analysis

Prior to spectral analysis, freeze-dried samples were milled at 50 revolutions per second for 3 min and diluted with IR transparent Potassium bromide (KBr). The samples were analysed with a Bruker Vertex 70 spectrometer equipped with a MCT (Mercury–Cadmium–Telluride) detector and a KBr beam splitter. Spectra resulting from 128 sample scans in a range from 3750 cm^{-1} to 400 cm^{-1} were produced with a resolution of 4 cm^{-1} . For the semi-quantitative analysis of LDPE and PET contents on bulk sediments, we used the calibration models by Hahn et al. (2019), which are based on synthetic sediment mixtures with defined microplastic contents.

Microplastic analyses were complemented using microscopy-assisted handpicking of plastic remains $>1\text{ mm}$. Classification is based on three semi-quantitative categories: 0 particles found, 1–2 particles found, and 3–10 particles found.

2.5. Diatom analysis

Eight surface sediment samples representing different parts of RBH were prepared for diatom analysis (Fig. 2). Samples were chemically treated with 30% H_2O_2 and 10% HCl. The resultant supernatant was sieved and swirled to remove coarser materials and sediments. The supernatant was then repeatedly suspended, allowed to settle over 8 h periods, and the excess water decanted, thus systematically removing finer particulates such as clay and concentrating diatom frustules in the

settled residue. Slides were mounted in Pleurax and diatoms were counted under a light microscope at up to $1000\times$ magnification. Identification of diatom species was based on diatom manuals and catalogues (Bate et al., 2004; Taylor et al., 2007).

2.6. Ostracoda and Foraminifera analysis

Aliquots from sediment samples for diatom analysis were also analysed for Ostracoda and Foraminifera (Fig. 2). The volume of each sediment sample was measured as a reference for the calculation of abundance. Samples were wet sieved (using tap water) through a $63\text{ }\mu\text{m}$ sieve and dried. A floating technique using a sodium polytungstate solution (Parent et al., 2018) was used to separate microfossils from clastic sediment. The recovery rate is about 96% (Semensatto and Dias-Brito, 2007).

For quantitative foraminifer and ostracod analysis, samples were dry sieved through $>200\text{ }\mu\text{m}$ and $125\text{--}200\text{ }\mu\text{m}$ mesh size sieves. The size fractions were split into sub-samples using a micro-splitter. Valves and tests from split samples were counted until 300 individuals of Foraminifera and Ostracoda for the $>200\text{ }\mu\text{m}$ fraction, and >200 foraminifer tests for the $>125\text{ }\mu\text{m}$ fraction were reached. All valves and tests were counted when the required number was not reached. Reworked individuals of both Foraminifera and Ostracoda were omitted from counts, e.g. those with abraded ornamentation or sediment inside the chambers. Ostracod carapaces were counted as two valves. Total abundance, diversity, and proportion of Ostracoda was calculated from the $>200\text{ }\mu\text{m}$

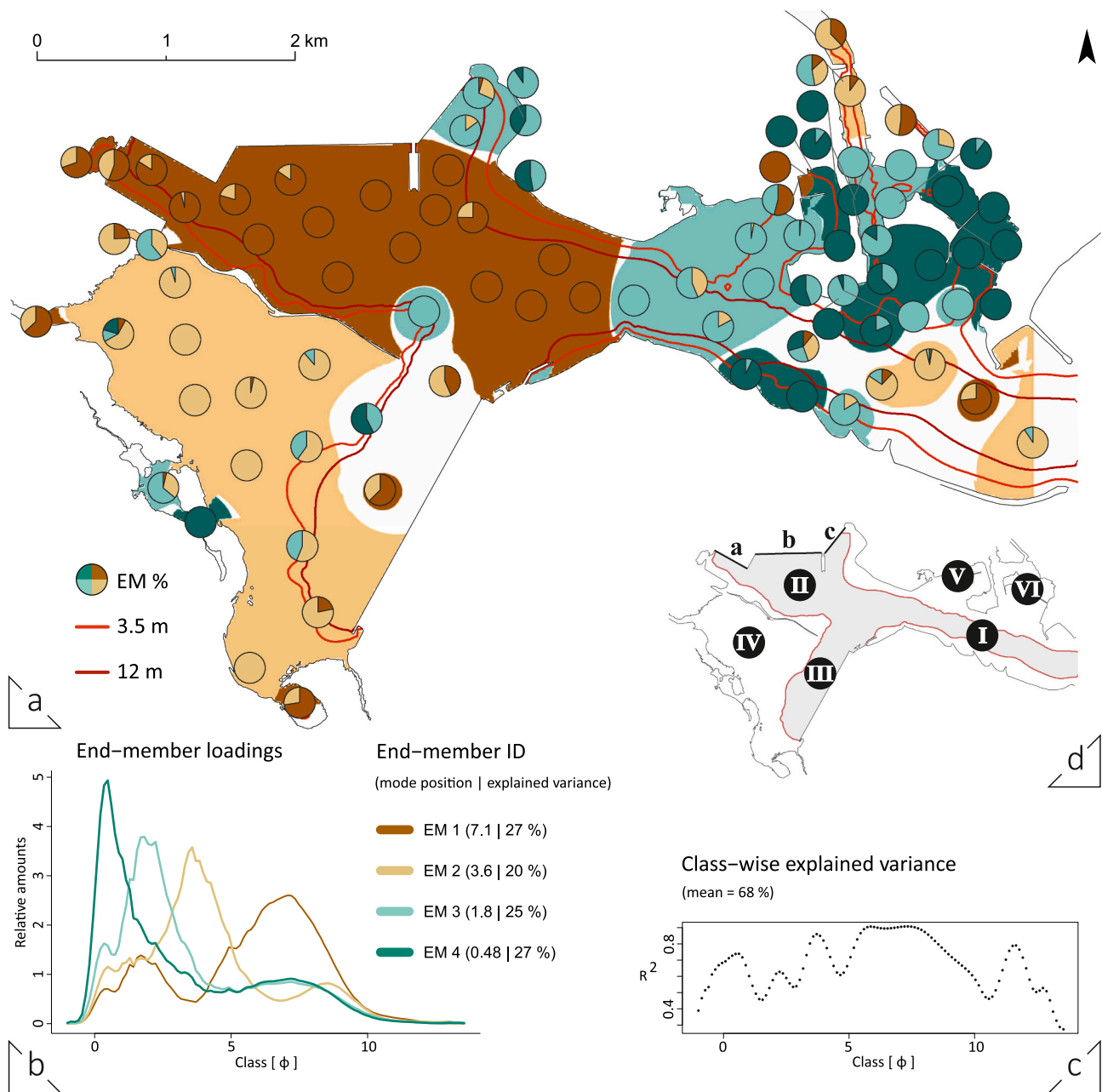


Fig. 5. a) Spatial distribution map of end-member scores (inverse distance weighting). Pie charts correspond to sample positions and detail the absolute end-member scores. Scores above 50% are coloured spatially. White areas indicate no dominant end-member score. Also indicated are the 3.5 and 12 m water depth contour lines. b) End-member loadings and explained variance. c) End-member class-wise explained variance. d) Sub-basin nomenclature. (For interpretation of the references to colour in this figure legend, the reader is referred to the web version of this article.)

size fraction count. Malformed foraminifera were counted separately in both size fractions to calculate a Foraminiferal Abnormality Index (FAI; Frontalini and Coccioni, 2008). Identification relied mainly on Benson and Maddocks (1964) and Dingle (1993, 1992) for Ostracoda, and Fürstenberg et al. (2017) and the World Register of Marine Species (<http://www.marinespecies.org/>) for Foraminifera. Species diversity was evaluated using Shannon's diversity (H') index (Shannon, 1948).

2.7. Core processing

Sediment cores (Table 1) were split in half, photographed, and lithologically described at the Physical Geography department of the University of Greifswald. Magnetic susceptibility was measured on split

cores using a Bartington MS2E point sensor (Bartington Instruments Ltd., Witney, UK) at 0.5 cm resolution. Core RBH18-12 and RBH18-23 were scanned with an ITRAX XRF-core scanner (COX analytical systems) at GEOPOLAR, University of Bremen. Sections were scanned with a Mo-tube with a step size of 2 mm, a count time of 20 s per step at a constant voltage of 30 kV, and a current of 50 mA. To account for matrix effects, data were normalized by total counts (element/kcps).

3. Results

3.1. Bathymetry and marine impact

RBH can be divided into six sub-basins (SB) (inset in Fig. 3), of which

Table 2
 Mean, Standard Deviation, minimum and maximum concentrations ($\mu\text{g g}^{-1}$, dry weight) for bulk sediments sampled in 2018 (analytical methods are indexed below element symbol: MS = ICP-MS, OES = ICP-OES).
 Guideline levels are given according to the Department of Environmental Affairs (2012b).

2018	Al	As		Ca		Cd		Co		Cr		Cu		Fe		K		Mg		Mn		Na		Ni		P		Pb		S		Sr		Ti		Zn		Rb	
		OES	MS	OES	MS	MS	MS	MS	MS	MS	MS	MS	MS	MS	OES	OES	OES	OES	OES	OES	OES	OES	OES	OES	OES	OES	OES	OES	OES	OES	OES	OES	OES	OES	OES	OES	OES	MS	MS
Min	4300	3	4841	0.1	2	11	2	4622	995	1776	100	1768	3	117	1	200	52	390	8	4																			
Max	72350	65	34241	1.5	25	969	67247	12625	13048	1495	31707	81	3125	49	9250	298	3582	274	90																				
Mean	30668	19	17388	0.2	12	169	31677	5612	580	580	580	10953	28	941	14	2635	130	1643	79	36																			
SD	20538	16	5831	0.3	6	172	16205	3641	320	3318	320	7987	18	704	9	2263	38	763	55	26																			
Warning Level		42		1.2		1.35/250						62/88			110																								
Level I		57		5.1		260						140			218																								
Level II		93		9.6		370						370			530																								

SB-I, -II, -III and V are dredged to maintain the operational water depth. As a result, the bathymetry clearly emphasizes marine traffic routes (Figs. 3, 4). Steep slopes (6-18°) – dredge scarps (Fig. 4c) – emerge towards the non-dredged sections, highlighted by the narrow separation of the 3.5 and 12 m water depth contour lines. Dredging operations scar the bottom and result in an uneven sediment surface (Fig. 4b). SB-II can further be subdivided based on proximity to three adjacent Dry- and Breakbulk terminals (a, b, c on inset in Fig. 3).

Salinities within RBH basins vary between about 34–35. The uniformly high salinity reflects tidal exchange with the Indian Ocean and limited inflow of freshwater. Lower salinities (30–31) occur north of Pelican Island (SB-VI, Fig. 3) and gradually decrease up Mzingazi Canal (reading 29), which connects RBH with the freshwater overflow of Lake Mzingazi (Fig. 1).

3.2. Grain-size distribution and end-member modelling

The steep bathymetric gradient formed by the dredge scarp is reflected in sediment granulometry. In general, the grain-size distribution in RBH reflects the bathymetry: mean grain-size (FWMphi; Folk and Ward, 1957) generally decreases with increasing water depth ($r = 0.71$, $p < 0.001$). Thus, deep basins SB-I, II and III – >12 m water depth – are dominated by silt, and shallower areas by sand.

Despite the positive correlation of surface sample mean grain-size and water depth, most grain-size distribution curves are bi- or trimodal. Therefore, in the deposited sediment, mean grain-sizes reference a value that condenses two or three modes (local maxima), individual grain-size fractions, and eventually sediment sources. End-member modelling statistically decomposes grain-size distributions and allows for a genetic interpretation. Here, end-member (EM) modelling was used (Dietze et al., 2014) to facilitate the use of grain-size as an environmental parameter and to distinguish the main detrital processes that contribute to sedimentation (Fig. 5).

Four significant end-members were identified from RBH surface sediment samples, which explain 68% of the variance of grain-size classes (Fig. 5c). The finest end-member, EM1, occurs mainly in SB-II and partially in SB-I and III (Fig. 5). The main constituent is fine silt (mode 7.1 ϕ , Fig. 5b), accompanied by a second fraction of medium to fine sand (mode 1.7 ϕ). Samples containing >50 vol% EM1 occur at an average water depth of 15 m, which is largely in sub-basins SB-I, II and III. In various samples, EM2 occurs with EM1. The majority of EM2 is in SB-IV, with a predominant grain-size of very fine sand (mode 3.6 ϕ) at an average water depth of 3 m. An array of less clustered samples is also classified as EM2 across much of RBH. EM3 occurs in various parts of the harbour, but predominates near the fairways at around 7 m water depth. Its main constituent is medium sand (mode 1.8 ϕ , Fig. 5b). The coarsest end-member, EM4, occurs in close relation to EM3 in shallower water areas (~1.5 m), mainly at the harbour entrance and along shorelines (Fig. 5a). EM4 is dominated by coarse sand (mode 0.5 ϕ , Fig. 5b).

3.3. Element concentrations in Richards Bay Harbour

The mean element concentrations in surface sediment sampled in 2018 follow the order Fe > Al > Ca > Na > Mg > K > S > Ti > P > Mn > Cr > Sr > Zn > Cu > Rb > Ni > As > Pb > Co > Cd (Table 2).

Apart from Ca, Cd, Sr and Ti, the elements (Table 2) correlate positively with one another. Aluminium (Fig. 14) is positively correlated with most elements ($r > 0.5$), bathymetry (Al/water depth; $r = 0.73$, $p < 0.001$) and mean grain-size (Al/FWMphi; $r = 0.95$, $p < 0.001$). Outliers – detected through geochemical normalization to Al – that in many cases reflect anthropogenic impact, alter the individual datasets, especially in the case of Cr and Cu. The removal of outliers results in an improved correlation to Al. Nevertheless, metal distribution patterns show significant spatial differences, despite their general correlation to Al.

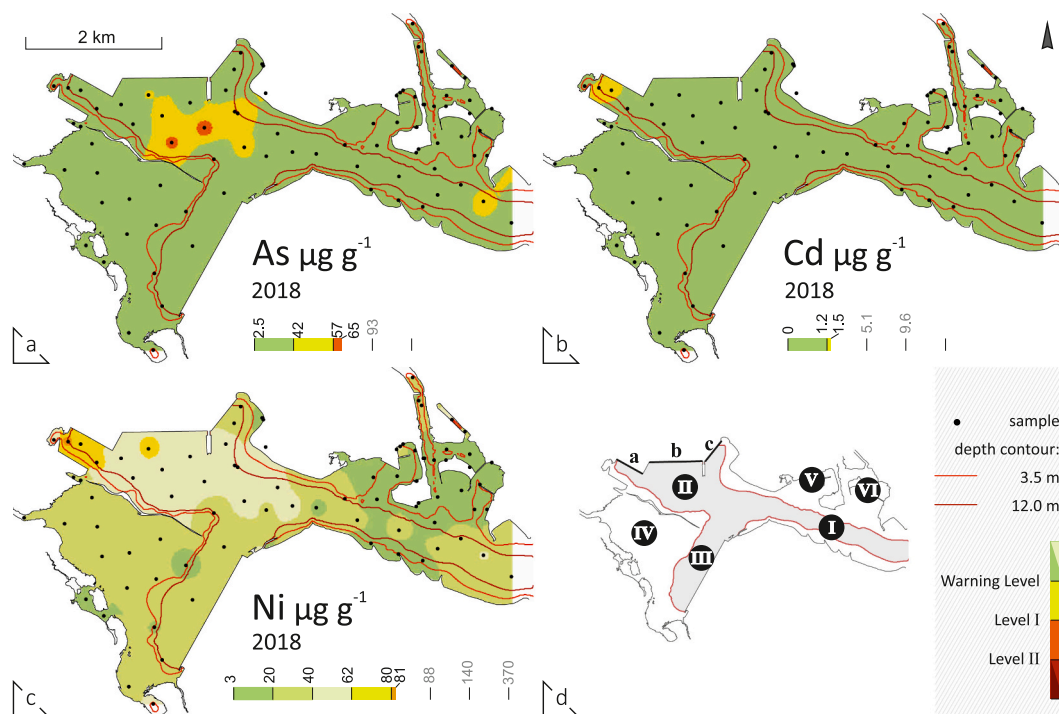


Fig. 6. Interpolated spatial distribution maps (inverse distance weighting) showing the concentration of As, Cd, and Ni. Each legend maxima refers to the guideline maxima (Department of Environmental Affairs, 2012b). Colour codes relate to guideline levels: $<$ Warning Level (green), $>$ Warning Level and \leq Level I (yellow), $>$ Level I and \leq Level II (orange), and $>$ Level II (red). d) Sub-basin nomenclature. (For interpretation of the references to colour in this figure legend, the reader is referred to the web version of this article.)

3.4. Trace metals – As, Cd, Cr, Cu, Ni

The highest concentrations of most trace metals, including As, Cd, Cu, Cr and Ni, which are of concern from a toxicological perspective, were in SB-II (Fig. 6). The highest concentrations of As were in the middle part of SB-II, farthest from quays, and is unlikely to reflect contamination (Fig. 6a). High concentrations of Cd, Cr, Cu and Ni were found in SB-IIa (Figs. 6 and 7). Sediment in SB-IIb contained high concentrations of Cr, Cu and Ni, while Cu and Cr were also at a high concentration in SB-IIc (Fig. 7).

3.5. 2018 Cr and magnetic susceptibility distribution

The range of Cr concentrations in sediment sampled in RBH was wide, from 11 to 968 $\mu\text{g g}^{-1}$ (Table 2, Fig. 7c). The lowest Cr concentrations were near the port entrance. Moderate concentrations were found mainly in SB-III, IV and V. The highest concentrations were in SB II, with a distinct increase in front of the bulk goods terminals (a, b, c on inset in Fig. 7f).

Low-field mass-specific magnetic susceptibility (χ_{LF}) values range from 0.15 to 4.48 $\cdot 10^{-6} \text{ m}^3 \text{ kg}^{-1}$, with consistently low values in SB-I, III, V and VI (Fig. 7e). Highest χ_{LF} values occur in front of the bulk goods terminals in SB-II and in the western part of SB-IV. Spatial magnetic susceptibility variations in surface sediment show similar patterns to Cr concentrations (Fig. 7c, e) and log-transformed datasets correlate positively (Cr Translog/ χ_{LF} Translog: $r = 0.71$).

3.6. Baseline models and Enrichment Factors

The Al normalized baseline models for Cr in sediment sampled in RBH in 2012 and 2018 are provided in Fig. 8, with baseline and enriched concentrations superimposed. Additional spatial distributions of Cr EF's

indicate only enriched sediment ($\text{EF} \geq 1$). Hereby both maps show strong similarities in their distribution pattern. However, during 2012 samples were taken very close to the northern pier in SB-II and indicate Cr enrichment towards the pile wall. While 2012 data ranges up to an EF of 3.0, considered high enrichment, 2018 data ranges up to an EF of 5.5, considered as severe enrichment (Fig. 8a, c).

3.7. Sediment cores

Core RBH18-12 (1.2 m) – collected in SB-II (Fig. 2) – can be divided into three units (I-III) from base to surface (Fig. 9). Unit I comprised an olive-green mud with black mackles. This gradually changed into unit II, a homogeneous olive mud with two intercalated sand layers. The top section (unit III) reverts to an olive-green mud with increasing number of black mackles. This subdivision can also be observed in low field magnetic susceptibility (κ_{LF}), Cr and Cu counts (Fig. 9). κ_{LF} and Cr show slightly lower values in unit II compared to unit I. However, both parameters show an increasing trend towards the top of unit III.

Sediment core RBH18-23 comprised an olive-green mud, with fine lamination and slight colour differentiation. The upper 23 cm were bioturbated and truncated by *Polychaeta* burrows. A subdivision into comparable units to RBH18-12 is not possible. Comparing the correlation factors between Cr/kcps and κ_{LF} of core RBH18-23 ($r = 0.8$) to core RBH18-12 ($r = 0.9$), a similar dependence and rise in both parameters is noticed, which confirms the previously detected relationship between χ_{LF} and Cr in surface sediments.

In contrast to Cr, highest Cu counts were evident in unit I and III of core RBH18-12, with spikes at 100–90 cm and 45 cm (Fig. 9). Similar to κ_{LF} and Cr, unit II had the lowest Cu counts. Cu counts were fairly constant through core RBH18-23.

A similar κ_{LF} pattern as that evident in core RBH18-12 was evident in cores RBH18-11 and -14, which form a NW-SE-transect in SB-II from the

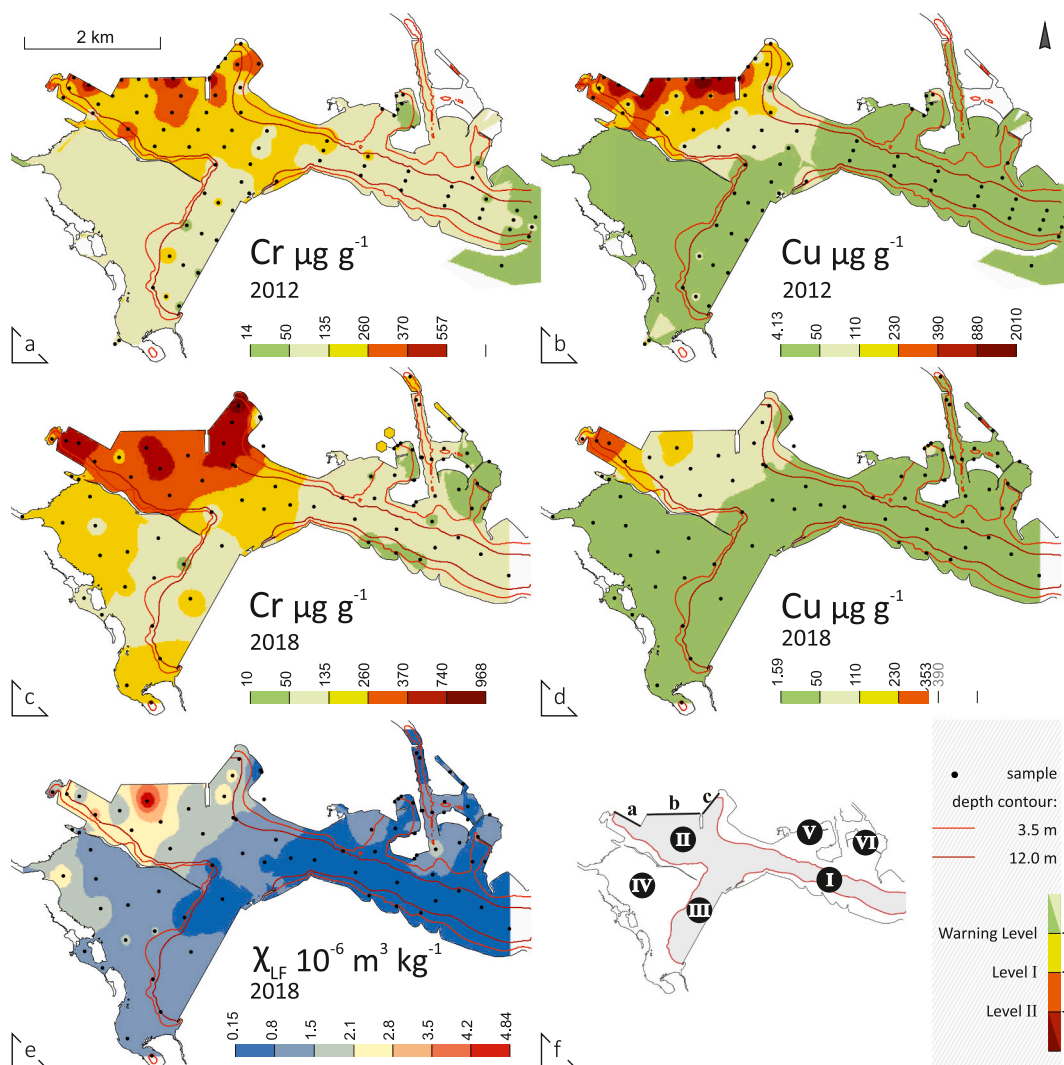


Fig. 7. Interpolated spatial distribution maps (inverse distance weighting) showing concentrations of Cr and Cu in 2012 (a, b) and 2018 (c, d). e) Pattern of magnetic susceptibility (χ_{LF}) measured in 2018. Colour codes resemble element concentration limits as indexed by the Department of Environmental Affairs (2012b): \leq Warning Level (green), $>$ Warning Level and \leq Level I (yellow), $>$ Level I and \leq Level II (orange), and $>$ Level II (red). f) Sub-basin nomenclature. (For interpretation of the references to colour in this figure legend, the reader is referred to the web version of this article.)

bulk terminal towards the middle of the harbour. Moving away from apparent Cr concentration maxima in SB-II (a-c), χ_{LF} decreases in surface sediment towards the SE (Fig. 7). This observation is also evident in the SB-II core-transect: κ_{LF} in the upper parts of the cores decreases from RBH18-11 to -14 (Fig. 10), the latter being furthest (about 1 km) from the bulk goods terminals (Fig. 2). Representative short cores from the western part of SB-IV, namely RBH18-23 and -25, also indicate increased κ_{LF} in regions of increased χ_{LF} in surface sediments (Figs. 2, 7, 9 and 10). In contrast, almost no magnetic susceptibility variation was evident in cores RBH18-10 and -21, which were at a greater distance from the bulk goods terminals (Fig. 2).

3.8. Microplastics

FTIRS analyses revealed two types of plastic in RBH sediment: polyethylene terephthalate (PET) and low density polyethylene (LDPE). PET was found in most samples. The highest abundances were nearest the port entrance (SB-I, SB-V and SB-VI) and near the coal terminal (SB-III) (Fig. 11). LDPE was found mainly in the SW part of RBH, in sediment

from SB-IV and small basins like SB-IIa and SB-V. The distribution of handpicked plastic pieces >1 mm visually resembles the PET-distribution, with higher abundances in SB-V. Correlation coefficients suggest a similar depositional behaviour of PET, EM4 ($r = 0.53$, $p < 0.001$) and medium sand ($r = 0.55$, $p < 0.001$).

PET and LDPE concentrations are negatively correlated ($r = -0.58$), and the individual distribution patterns visually oppose one another (Fig. 11). Therefore, the predominant occurrences can be assigned to different harbour sub-basins.

3.9. Bioindicators

The Foraminifera Abnormality Index (FAI) ranged between 0 and 9.1 for samples with at least 40 counted foraminifer tests (Table 4). Most samples contained high abundances of microfossils, mostly in good preservation, for all three groups. Exceptions were samples #62 and #64 directly in front of the bulk goods terminals in SB-II (SB-IIc and SB-IIa), where diatoms, foraminifers and ostracods showed low abundances and were often fragmented or poorly preserved. Foraminifera and

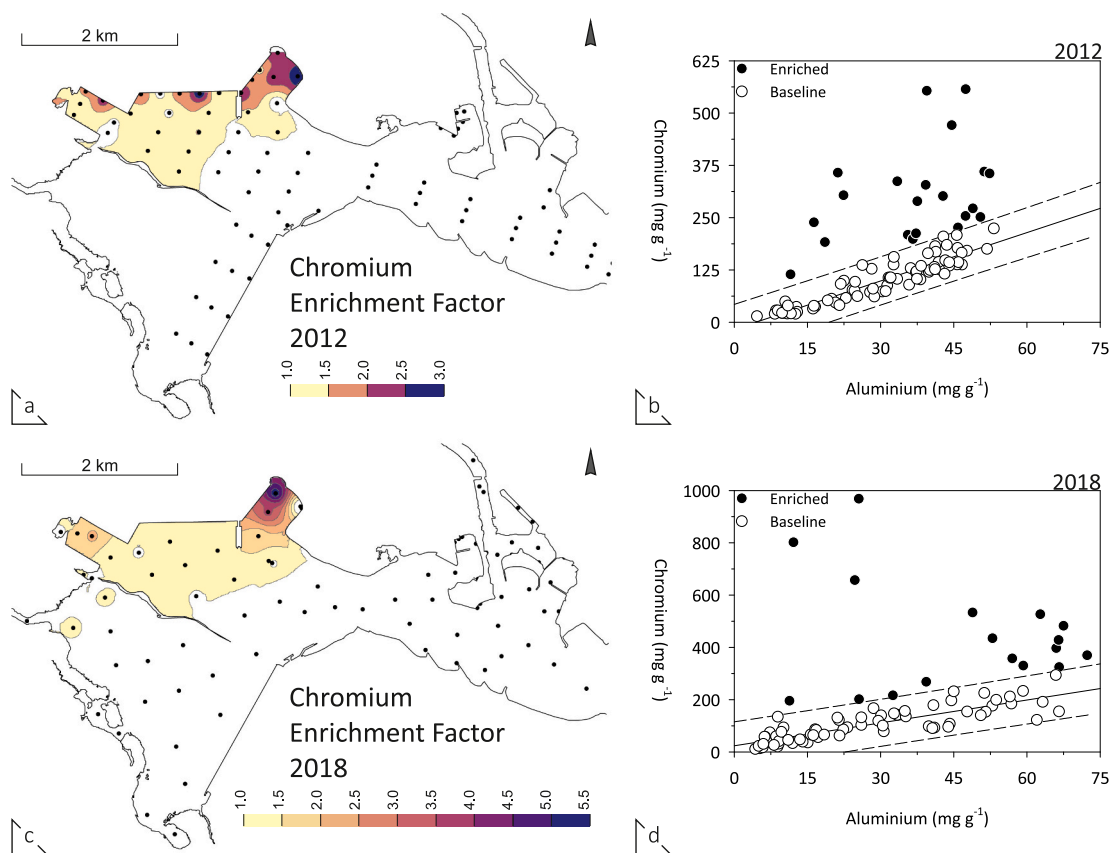


Fig. 8. Baseline models for Cr in surficial sediment sampled in Richards Bay Harbour in 2012 (b) and 2018 (d), enriched samples are black dotted. Associated spatial distribution maps (a, b) of Enrichment Factors (EF), interpolated via inverse distance weighting, are coloured if $EF \geq 1$, whereby we categorize: low ($EF \geq 1-1.5$), moderate ($EF > 1.5-2.5$), high ($EF > 2.5-5$), and severe ($EF > 5$) enrichment.

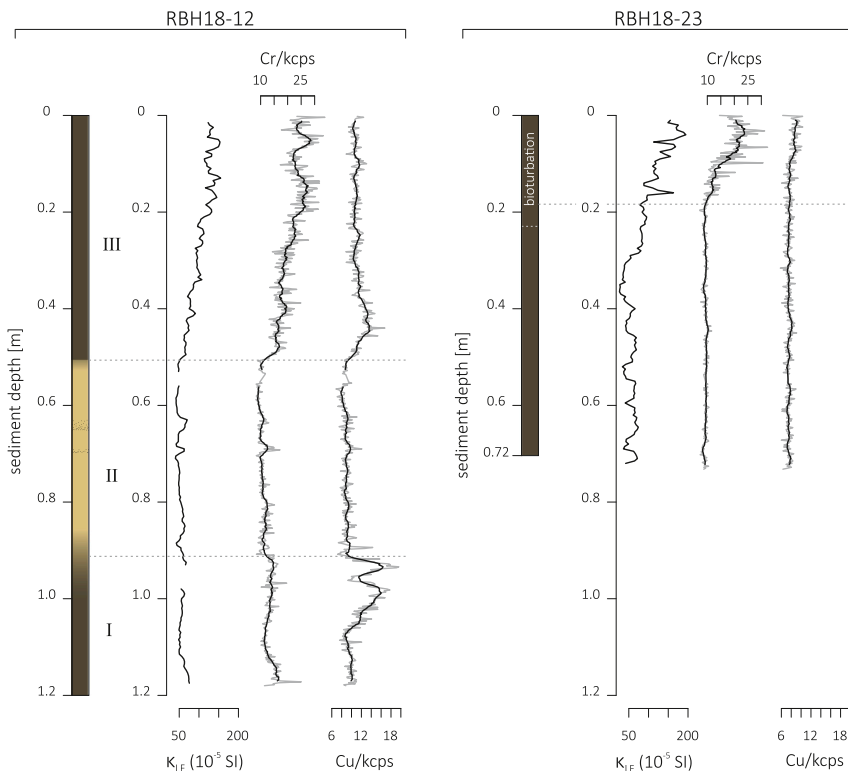


Fig. 9. Lithology, magnetic susceptibility and normalized XRF counts for Cr and Cu (grey line = original data at 2 mm resolution, black line = moving average (11 periods)) from sediment cores RBH18-12 and -23.

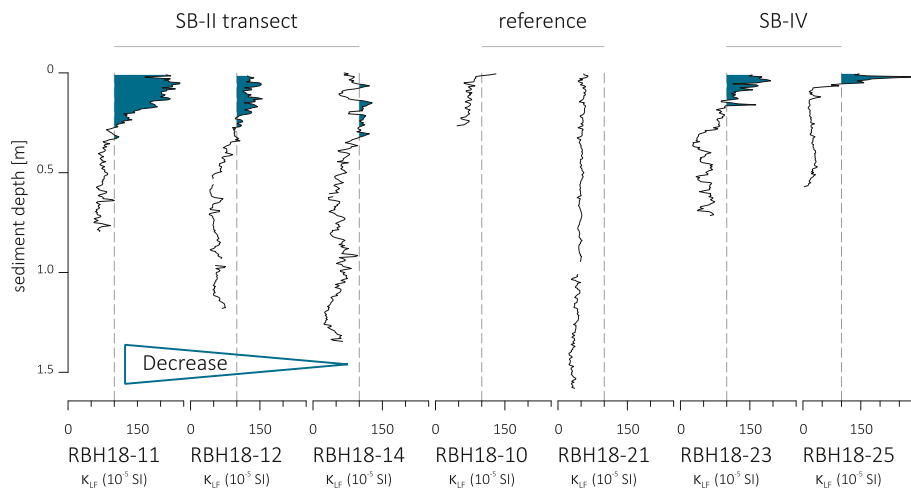


Fig. 10. Low field magnetic susceptibility (κ_{LF}) of selected sediment cores. All measurements are plotted on the same scale. Note the reference line at $100 \cdot 10^{-5}$ SI. Left: transect RBH18-11 to -14 indicates a decrease in susceptibility (with increasing distance from bulk terminals). RBH18-23 and -25 from SB-IV indicate comparable values to the transect. Reference cores RBH18-10 and -21 in which κ_{LF} is below $100 \cdot 10^{-5}$ SI. For core locations see Fig. 2.

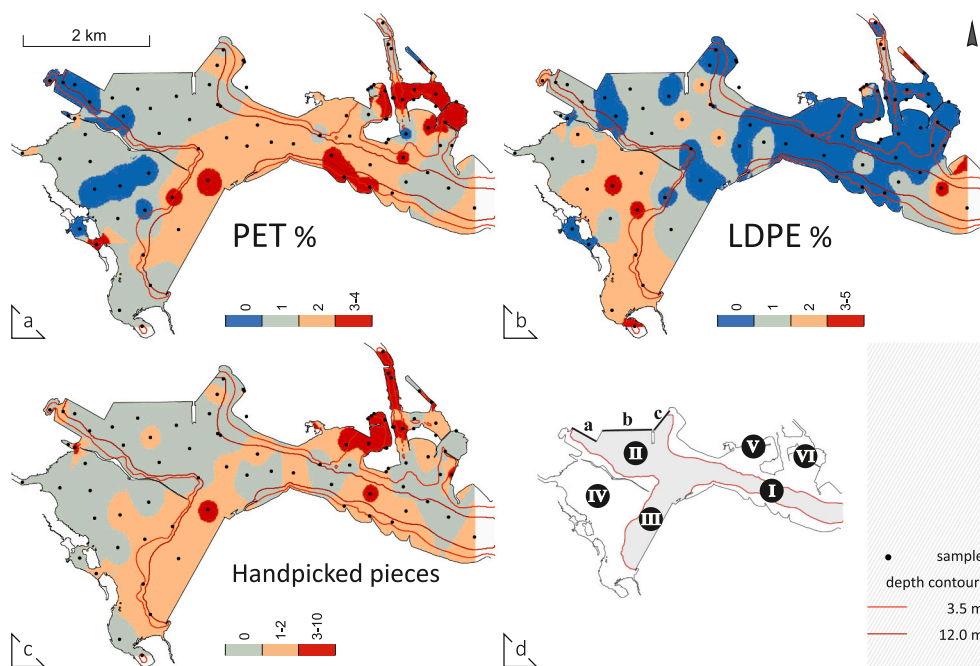


Fig. 11. Distribution maps of FTIRS spectroscopy inferred a) PET%, b) LDPE% and c) handpicked plastic pieces, interpolated by inverse distance weighting. Handpicked pieces refer to a categorical system (numbers identify pieces found; adopted from Schell, 2019). d) Sub-basin nomenclature.

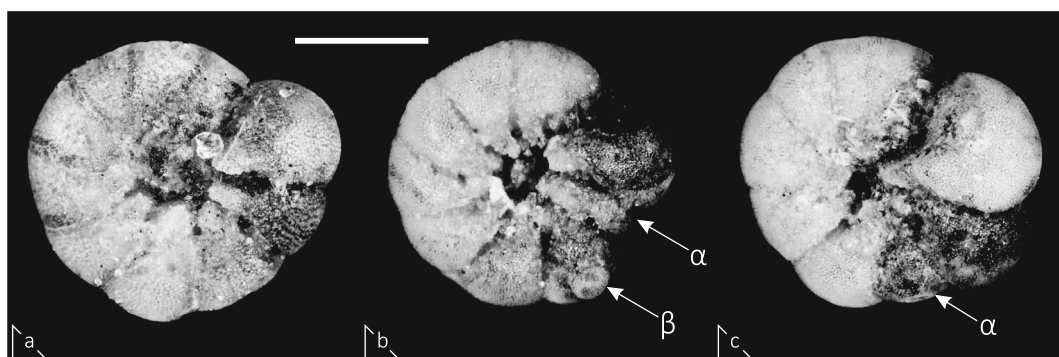


Fig. 12. Umbilical views of a) normal and b), c) malformed tests of *Ammonia* sp. from sample TR18-62, Richards Bay. The arrows point to malformation features such as dwarf chambers (α) or an accessory chamber (β). Scale bar = 200 μ m.



Fig. 13. Left: Historical aerial image of Richards Bay Harbour during construction (© Klaus Jost – jostimages.com). Intensive sand (light brownish areas) relocation occurred during construction. The majority of sand features were temporary and do not exist today. Note that North is to the right. Right: Resuspension of surface sediment via berthing procedures at SB-II (source Google Earth). Sediment clouds – caused by propellers near to the seafloor – are often visible on aerial images.

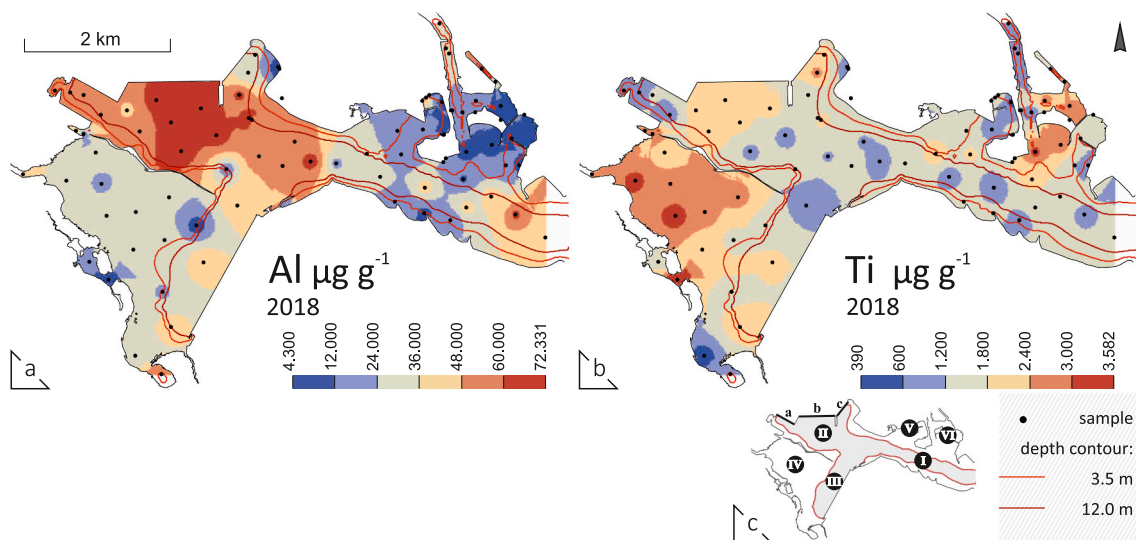


Fig. 14. Spatial distribution maps of a) Al and b) Ti, interpolated with inverse distance weighting. The elemental concentrations indicate a strong difference in accumulation patterns. c) Sub-basin nomenclature.

Table 3

Mean, Standard Deviation, minimum and maximum concentrations ($\mu\text{g g}^{-1}$, dry weight) for bulk sediments sampled in 2012 (analytical methods are indexed below element symbol: MS = ICP-MS, OES = ICP-OES). Guideline levels are given according to the Department of Environmental Affairs (2012b).

2012	Al	As	Ca	Cd	Co	Cr	Cu	Fe	K	Mg	Mn	Na	Ni	P	Pb	S	Sr	Ti	Zn	Rb
	OES	MS		MS	MS	MS	MS	OES			OES	OES	MS		MS				MS	
Min	4665	1	–	0.0	2	14	4	3959	–	–	76	–	2	–	2	–	–	–	8	–
Max	53219	22	–	8.9	95	557	2016	55657	–	–	4746	–	1836	–	639	–	–	–	605	–
Mean	31494	9	–	0.4	14	143	117	30884	–	–	506	–	64	–	22	–	–	–	94	–
SD	13052	5	–	1.2	10	110	256	13772	–	–	489	–	186	–	64	–	–	–	87	–
Warning Level		42		1.2		135/250	110						62/88		110				270	
Level I		57		5.1		260	230						140		218				410	
Level II		93		9.6		370	390						370		530				960	

Ostracoda showed a general low diversity, and in particular *Ammonia* sp. showed malformations (Fig. 12) with an FAI of 4.2% and 5.1% for these two positions, respectively.

Sample #72 contained an abundant and well preserved diatom flora and a low to moderate number of calcareous microfauna, dominated by ostracods (Table 4). Similarly, sample #4 showed a low diversity of calcareous microfossils, a clear dominance of ostracods, and a very high FAI. Calcareous microfauna in sample #39 were virtually non-existent.

Within SB-IV, sample #47 showed a very high FAI (based on low counts) and a clear dominance of ostracods. Sample #50 showed the highest abundance of calcareous microfauna, with a slightly elevated FAI and ostracod dominance (Table 4). Sample #33 yield a well-preserved, rich diatom flora, while Ostracoda and Foraminifera showed a low abundance but a high diversity and the lowest FAI of the dataset (Table 4).

Table 4

Bioindicator data from RBH in 2018. Values in bold point to ecological stress; brackets are based on low counts. FAI = Foraminifer Abnormality Index; n.a. = not applicable. SB = sub-basin. Cr concentration is provided for comparison.

Sample TR18-	Cr [$\mu\text{g g}^{-1}$]	Diatoms		Foraminifera and Ostracoda				SB
		Number of species	Abundance and preservation	Abundance [spec./100 ml]	Diversity (Shannon H')	Ostracoda [%]	FAI [%]	
4	185	68	Good	520	0.7	96	9.1	V
33	98	58	Good	118	1.9	5.3	0	I
39	233	78	Good	1	n.a.	n.a.	n.a.	III
47	197	–	Good	382	1	96.7	[33.3]	IV
50	140	65	Good	5729	1.4	60.4	2.1	IV
62	969	33	Poor	294	0.8	16.3	5.1	II-c
64	435	37	Poor	598	1.6	58	4.2	II-a
72	428	–	Good	255	1.1	75.8	n.a.	II

4. Interpretation

4.1. Sediment dynamics

Similar to mean grain-size, EM1 to EM4 indicate an increase in grain-size with a decrease in water depth. A distinct gap between mode positions of EM1 (7.1 ϕ ; fine silt) and EM2 (3.6 ϕ , very fine sand) emphasizes a strict boundary between the two accommodation spaces (Fig. 5b). This is associated with the most prominent effect of dredging operations – the maintained steep depth gradient. Further, reoccurring dredging operations remove surficial sediments. However, the clustering of samples with a dominating end-member score (>50 vol%) in distinct areas and water depths of RBH indicates a non-random depositional pattern (Fig. 5). Therefore, we assume a stable accumulation space during the time of sampling. A second mode in the grain-size distribution curve of EM1 (Fig. 5b, also apparent in EM2 and EM3) represents an input of clastic material from a separate source. Marine operations, including traffic and propeller-induced sediment suspension (Fig. 13), probably affect the redistribution of sediment (end-members). EM2, outside of SB-IV, is process related and indicates downslope fining along fairways. EM4 represents tide-influenced shallow water conditions. This is in agreement with previous observations in which the sedimentary load deposited in coastal areas reflected a strong influence of longshore transport of beach sands, especially those deposited at the harbour entrance (Schoonees et al., 2006).

The predominance of EM4 in SB-VI, which is coupled to the occurrence of sand within the harbour sediments, might be related to intensive sand relocation during the construction phase of the harbour, which can be observed in historical aerial images (Fig. 13). At that time, construction material (according to our results probably mainly sand) was dumped to the north of the harbour entrance directly adjacent to SB-V and VI.

4.2. Al and Ti

Commonly used minerogenic input indicators are Al (Haberzettl et al., 2019; Strobel et al., 2019; Wüdsch et al., 2016) and Ti (Haberzettl et al., 2009; Haberzettl et al., 2005; Kasper et al., 2012) (Fig. 14). The low correlation between Al and Ti is surprising at first, but can be explained by the surrounding geology. Ti is a major component of surrounding dune sands, which contain large amounts of heavy minerals and are mined nearby for ilmenite, rutile and zircon (Williams and Steenkamp, 2006). Density differences in minerals containing Ti and Al likely result in different transport and deposition processes. The highest Al concentrations were found in deeper water of SB-I, II and III. Ti was observed in higher-energy shallow water areas (Fig. 14b). As most other elements correlate positively to Al, we expect their distribution to depend on grain-size and the respective hydrodynamic regime in which they are deposited. This relationship between the spatial distribution of trace metals and grain-size has been often recognized (Förstner and

Wittmann, 1981) and has been observed in comparable studies (Haberzettl et al., 2019; Haberzettl et al., 2010; Ohlendorf et al., 2014).

4.3. Cr and magnetic susceptibility distribution

Magnetic susceptibility is influenced by various factors, such as different mineralogical compositions, concentrations of magnetic minerals, and their magnetic grain-size and morphology (Ellwood et al., 2007; Haberzettl, 2015; Hatfield et al., 2013; Lisé-Pronovost et al., 2013). RBH has a low underlying magnetic susceptibility pattern that relates to a marine influence, which is larger at the harbour entrance. Marine sediments are usually enriched in diamagnetic minerals such as carbonates, and hence yield lower magnetic susceptibility values. The distinct increase in the magnitude of magnetic susceptibility and Cr concentration, which itself has a strong positive susceptibility (Dearing, 1994), in SB-II (front of the bulk goods terminals) indicates an additional input of Cr. This is likely associated with a point source rather than a hydrodynamic distribution.

4.4. Temporal pollution variations in sediment cores

The lowest Cu and Cr concentrations and magnetic susceptibility values in the lowermost part (lower part of unit I) of sediment cores RBH18-12 and RBH18-23 are assumed to reflect natural background conditions. The spike in the Cu concentration in the upper part of unit I in core RBH18-12, which is continued in the lower part of unit III (Fig. 9), indicates an additional, probably anthropogenic, Cu contribution.

We hypothesize that unit II of sediment core RBH18-12 consists of reworked material due to the distinctly different characteristics seen in all parameters (Fig. 9). Dredging activities might have caused a disturbance or reworked material. The susceptibility (and Cr and Cu concentration) is identical to lower unit III, and therefore comparable to the assumed background concentrations for the sediment characteristic of this core.

Progressively decreasing concentrations in the upper 40 cm reflect a decrease in Cu deposition towards the present time. At the same time, Cr and magnetic susceptibility increased in the recent past. Excluding the hypothesized reworked sediments of unit II, this spike in the Cu concentration and the increasing Cr concentration in sediment core RBH18-12 accords with the history of products exported through RBH. Copper ore was exported through the port until 2012. The abrupt increase in Cu concentrations (Fig. 9) in core RBH18-12 at around 100 cm sediment depth might indicate the onset of Cu ore export. Correspondingly, the return to lower levels at about 30 cm could represent the end of Cu export. However, Cu concentrations have not returned to background concentrations, probably reflecting residual contamination (Fig. 9). Comparing spatial distributions of Cu from 2012 to 2018 (Fig. 7), a decreasing trend is evident and the mean Cu concentration (Table 3) was about a third lower in 2018.

Table 5

Sediment quality guideline quotients (min, max and median) for individual metals, and the mean sediment quality guideline quotient for sediment sampled in the Port of Richards Bay in 2012 and 2018.

	As	Cd	Cu	Cr	Ni	Pb	Zn	Mean quotient
2012								
Minimum	0.01	0	0.01	0.04	0.01	0	0.01	0.01
Median	0.09	0	0.09	0.33	0.1	0.03	0.08	0.11
Maximum	0.24	0.92	5.17	1.5	4.96	1.21	0.63	1.69
2018								
Minimum	0.03	0	0	0.03	0.01	0	0.01	0.01
Median	0.15	0	0.05	0.32	0.07	0.02	0.07	0.12
Maximum	0.7	0.16	0.91	2.62	0.22	0.09	0.29	0.47

In contrast, Cr ore and ferrochrome are currently exported in high volumes through the harbour. The ore and ferrochrome are temporarily stored at open-air sites. Continuously increasing Cr concentrations in unit III (Fig. 9) possibly mirror increasing export volumes at the bulk goods terminal. Spillage during loading or strong winds could explain localized high Cr concentrations that decrease with distance from the source (bulk goods terminal). During the 2012 field campaign, ferrochrome nuggets were found in sediment samples collected in SB-IIb (Fig. 15).

The positive correlation between Cr concentration and χ_{LF} in RBH surface sediments and between Cr counts and κ_{LF} in cores RBH18-12 and -23 allows the use of magnetic susceptibility (κ_{LF}) – measured on all cores – as a measure of Cr contamination in the cores (Fig. 10). The decreasing intensity in magnetic susceptibility in the sediment core transect RBH18-11 to -14 (Fig. 10) (especially at the upmost core-sediment) is similar to the modern surface distribution of Cr (Fig. 7), which indicates a decreasing trend with distance from the pollution source.

SB-IV is a restricted access area and in a more natural state (cf., bioindication). However, industrial runoff – linked to aluminium smelters and a fertilizer- and phosphoric acid plant in the surrounding – that enters upstream of Bhizolo Canal (cf., Fig. 1 for location) is responsible for contamination (Wepener and Vermeulen, 2005). While this might indeed be an explanation, we additionally recognize a similarity in the sediment cores – RBH18-12 and -23 – both showing an increased Cr content and susceptibility towards present sediment (Fig. 9). Therefore, we hypothesize a redistribution of fine particles by tidal currents, wind forcing or vessel propeller wash (Fig. 13) from SB-II via a small passage (Fig. 3) in the northeast of SB-IV and a distribution across SB-III during incoming tides.

4.5. Microplastics

The highest concentrations of PET or handpicked plastic pieces >1 mm were in sediment in public parts of RBH, especially at a beach in SB-VI. Recreational use of these beaches is high, particularly in summer, and the PET accumulation undoubtedly reflects plastic litter entering the harbour. Handpicked microplastic pieces were located predominantly in the Small Craft Harbour (restaurant and business area, and a popular bathing beach) of SB-V and along private jetties in Mzingazi Canal. Despite a slight difference in distribution patterns, PET and handpicked microplastic pieces show a clear link to areas of pronounced human use in the harbour.

Due to the high density of PET (1.33–1.41 g cm⁻³; Fath, 2019) relative to seawater (~1.02 g cm⁻³; Nayar et al., 2016; Sharqawy et al., 2010), PET particles likely sink to the bottom (Bellasi et al., 2020; Fath, 2019). Additionally, the density of PET enables preferential deposition within higher energy areas, explaining correlations to EM4 and medium sand. Lower energy transportation processes reduce the occurrence of PET and plastic pieces >1 mm towards inner basins of RBH (SB-IIa-c, SB-IV). However, PET particles still accumulate in lower energy, deep water areas that are affected by tidal currents and marine traffic induced

currents and turbulence (Fig. 13).

Due to the density difference to seawater, Low Density Polyethylene (LDPE; 0.88–0.98 g cm⁻³; Fath, 2019) has a tendency to float (Corcoran, 2015). Thus, current mediated transport occurs over a wider area, leading to LDPE accumulation in remote areas such as in SB-IIa, and at sites #4, #39 and #50 (Figs. 11, 2). To meet settling conditions certain factors are necessary (Bellasi et al., 2020; Corcoran, 2015; Fath, 2019), with biofouling being a compelling process. Based on the higher LDPE appearance in isolated basins (e.g. SB-IV, sites #39 and #50), isolated calm water conditions should also be preferential for deposition. The marine fairways were almost LDPE-free. LDPE appears mainly in the SW part of the harbour in SB-IV, and possibly relates to the main wind directions NE-SW (Begg, 1978). Surface waters would carry LDPE from their possible source (SB-V, VI) towards the SW. However, once settled, opposing wind turbulences towards NE will not redistribute the same amount. In addition, PET and handpicked remains preferentially occur in SW SB-III, which also underlines the influence of the prevailing wind from the NE.

Simultaneously, the individual distribution patterns of PET and LDPE indicate effects of hydrodynamic control in close relation to their density and resulting accumulation space. Reorganization of particles due to the prevailing wind direction, tidal currents and marine traffic-induced turbidity are considered plausible.

4.6. Bioindication

We used three taxonomic groups (diatoms, foraminifers and ostracods) as bioindicators to focus on effects of detected metal contamination in selected samples. This shortened approach is a reconnaissance study to test the abundance, species diversity, relative proportion of ostracods, and malformations in foraminifer tests. It is noteworthy that, according to our study, metal contamination, and especially Cr and Cu, enters RBH in the residual fraction, which is known to be less bioavailable (Sah et al., 2019). Based on investigations of all three groups we conclude that an increased level of metal contamination has adverse effects on the selected taxa, but affects them at a group level to different degrees and lowers the diversity in favour of opportunistic species. Hereby, diatoms and foraminifers seem to be more affected than ostracods. Generally, ostracods show higher abundances at severely metal contaminated sites, such as #47, #62 and #64. Ostracoda seem to have a greater physiological tolerance to elevated metal concentrations (Millward et al., 2004) and therefore dominate the calcareous microfauna under these conditions.

We interpret the moderate representation of opportunistic species at sites #47, #64 and #72 as a relatively recent pollution event. Additionally, the strong appearance of the diatom taxon *Fragilaria tenera* at site #72 is indicative of an incipient contamination event (Cattaneo et al., 2004). The highly fragmented nature and low concentrations of diatoms at site #62, correlating to the Cd warning level, may be evidence of negative effects of the metal on photosynthesis, resulting in reduced primary productivity and thus reproduction (Marshall and Mellinger, 1980).

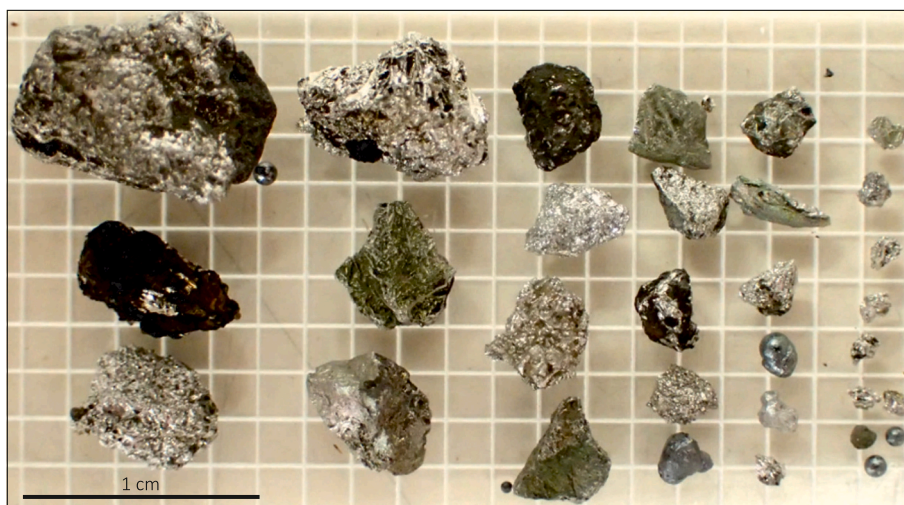


Fig. 15. Assorted ferrochrome particles of various sizes (gravel to fine sand) from 2012 survey samples collected in SB-IIb.

Ostracod proportions and FAI at the entrance to the Bhizolo Canal (site #47) appear very high, suggesting metal pollution. The rise in metal pollution at site #47 introduces diatom species, such as *Navicula salinicola*, that have been shown to propagate under increased metal and nutrient concentrations (Belando et al., 2017), while *Halamphora coffeaeformis*, which reaches its greatest representation at this site, is known to be tolerant of increased concentrations of metals such as zinc (Nguyen-Deroche et al., 2012).

The relatively low level of anthropogenic disturbance is seen at site #50 in SB-IV, which is separated by a sand barrier and thus more distal to pollution sources in SB-II (Figs. 2, 7). The highest diversity of calcareous microfossils at site #33 is likely due to the strong marine influence and also the least contaminated area relative to pollutants measured in our study. Frequent sediment reworking by tidal currents and vessel passage may also explain the low abundance of species. This hydrodynamic setting at site #33 can be inferred from the diatom community, which has a greater proportion of brackish-marine tycolanktonics responding to high-energy coastal processes (Kirsten et al., 2018).

5. Discussion

5.1. Comparison of elemental distribution to guidelines

The South African Department of Environmental Affairs uses a National Action List to screen sediment identified for dredging in South African ports (Department of Environmental Affairs, 2012b). There are three guidelines for various metals: The Warning Level indicates an early stage of contamination, but is not used for decision-making. Action Level I and Level II are used for decision-making. Based on these guidelines, we highlight concentration thresholds of As, Cd, Cr, Cu, Ni and Zn (Figs. 6 and 7). The As concentrations exceed Action Level I in the middle harbour area, while the Cr and Cu concentration exceed Level I and Level II. The highest Cr and Cu concentrations in RBH exceed the Level I by a factor of >3.5 ($968 \mu\text{g g}^{-1}$ vs $260 \mu\text{g g}^{-1}$) and >1.5 ($353 \mu\text{g g}^{-1}$ vs $230 \mu\text{g g}^{-1}$), respectively (Fig. 7, Table 2). The mean Cr concentration in sediment near the terminal in SB-II is alarmingly high, at $351 \mu\text{g g}^{-1}$, and in 42% of samples here exceed Level II. The Cr concentration in 45% of samples collected in 2018 (Fig. 7) was above the Warning Level ($\text{Cr} > 135 \mu\text{g g}^{-1}$), providing an aerial coverage of about 6.5 km^2 . Additionally, the onset of increasing magnetic susceptibility (which correlates positively with Cr, Fig. 8) within the sediment core transects (Fig. 10) shows significant contamination in the top 30 cm of sediment. This results in an estimated volume of $1,950,000 \text{ m}^3$ of

sediment with an elevated Cr concentration in RBH, which should be considered in future dredging operations and sediment disposal at the open water disposal site in the Indian Ocean.

5.2. Ecotoxicological implications

The ecological risk posed by As, Cd, Cr, Cu, Ni, Pb and Zn in sediment can be estimated using the sediment quality guideline quotient (SQGQ) approach (Long et al., 2006). The concentrations of these metals are divided by the Level II of the sediment quality guidelines defined by the Department of Environmental Affairs (2012b). For several of the metals these sediment quality guidelines are similar to the Effects Range Median (ERM) of the sediment quality guidelines derived by Long et al. (1995). As a further estimate of the risk for multiple metals in sediment, the mean sediment quality guideline quotient (mSQGQ) was calculated as the mean of the quotients for individual metals in each sediment sample.

The mSQGQ for surface sediment sampled in 2012 ranges from 0.01–1.69 (Table 5), indicating a risk of toxicity by metals in some samples. However, the median mSQGQ value of 0.11 shows a low risk of toxicity at most samples. Quotients >0.5 are exclusively for sediment in SB-II, near terminal operations. The highest individual SQGQs indicate severe contamination for Cu, Ni and Cr, at 5.17, 4.96 and 1.50 respectively. The mSQGQ for sediment sampled in 2018 ranges from 0.01–0.47 (Table 5), with a median of 0.12. The highest SQGQs, as for the 2012 survey, were calculated for sediment sampled in SB-II, at 0.91 and 2.62 for Cu and Cr respectively.

5.3. Comparison to earlier studies

In this section, we make use of and compare absolute maximum values from different surveys to metal concentrations in surface sediment in our study from RBH, noting that the strong dependence between elemental concentrations and grain-size distributions detracts somewhat from such comparisons.

A summary of concentration ranges for Al, Cu, Cr, Fe, Mn and Zn in studies dating back to 1976 is compiled in Wepener and Vermeulen (2005), indicating lowest Cu and Cr concentrations in sediment of $40 \mu\text{g g}^{-1}$ (Cloete, 1979) and $74.8 \mu\text{g g}^{-1}$ (Oliff and Turner, 1976), respectively in 1976 surveys. During their 1996–1997 survey's, Wepener and Vermeulen (2005) indicate an increase in concentrations: maximum concentrations for Cu ($53.5 \mu\text{g g}^{-1}$) and Cr ($221.9 \mu\text{g g}^{-1}$). These are already above present guidelines (Department of Environmental Affairs, 2012b) and are further exceeded in samples collected in 2012 (Cu $2016 \mu\text{g g}^{-1}$;

Cr 557 $\mu\text{g g}^{-1}$) and 2018 (Cu 353 $\mu\text{g g}^{-1}$; Cr 969 $\mu\text{g g}^{-1}$).

Greenfield et al. (2011) and Wepener and Degger (2020) identified increased metal concentrations in the tissue of mussels (*Perna perna*) from buoys near Naval Island in 2008 and 2009. Compared to 2008, mussels of the 2009 survey show a decrease in Cu and an increase in Cr concentrations. This change, over the course of one year, is similar to anomalies in the sediment core XRF data, where a decreasing trend of Cu is accompanied by an increase in Cr (Fig. 7).

Wepener and Vermeulen (2005) relate temporal spikes in metal concentrations to activities like dredging, which cause a disturbance in oxic and anoxic conditions. However, the spatial distribution patterns in 2012 and 2018 indicate point sources on globally dredged surface sediment and cores RBH18-12 and -23 confirm the constant deposition of metals in sediment.

5.4. Regional comparison

In order to set the results in a regional context, we compare the results for RBH to ports in East London and Port Elizabeth in South Africa as presented in Fatoki and Mathabatha (2004). Maximum Pb concentrations in all three ports are below Warning Levels (Department of Environmental Affairs, 2012b), at 82.2 $\mu\text{g g}^{-1}$ in East London, 61.9 $\mu\text{g g}^{-1}$ in Port Elizabeth, and 48.8 $\mu\text{g g}^{-1}$ in RBH. Maximum Zn concentrations in East London (332 $\mu\text{g g}^{-1}$) and RBH (274.2 $\mu\text{g g}^{-1}$) were above, and in Port Elizabeth (126 $\mu\text{g g}^{-1}$) below the Warning Level. Maximum Cd concentrations surpass the Warning Level in all ports (Port Elizabeth 1.4 $\mu\text{g g}^{-1}$, RBH 1.5 $\mu\text{g g}^{-1}$, East London 1.63 $\mu\text{g g}^{-1}$).

In contrast, maximum Cu concentrations in RBH are twice as high compared to East London and four times higher than in Port Elizabeth (RBH: 353.4 $\mu\text{g g}^{-1}$, East London: 183 $\mu\text{g g}^{-1}$, Port Elizabeth: 92.5 $\mu\text{g g}^{-1}$; Fatoki and Mathabatha, 2004). Fatoki and Mathabatha (2004) present site-specific annual mean Cu concentrations in sediments at the Port Elizabeth Cruise Terminal and East London motor vehicle berth of 68.5 $\mu\text{g g}^{-1}$ and 106 $\mu\text{g g}^{-1}$ Cu, respectively. The mean Cu concentration of 88.6 $\mu\text{g g}^{-1}$ at RBH dry and breakbulk berths (SB-II) compares well to these findings. In this regard, local similarities, like surrounding industrial runoff and marine operations (ship maintenance), are likely the main contributors for elevated Cu concentrations at all three sites.

Birch et al. (2020) recently assessed sediment metal enrichment in ten ports and estuaries in the World Harbours Project. Concentrations found in RBH for Cr and Cu differ considerably to those reported by Birch et al. (2020). Cr concentrations in RBH exceed concentrations reported for sites by Birch et al. (2020) by a factor of 3.1 (overall harbour mean: 54 $\mu\text{g g}^{-1}$ and overall maximum 316 $\mu\text{g g}^{-1}$, Table 2). Mean Cu concentrations in RBH are below the average of 51 $\mu\text{g g}^{-1}$ (Birch et al., 2020), but maximum Cu concentrations in RBH (353 $\mu\text{g g}^{-1}$) are above the average maximum of 237 $\mu\text{g g}^{-1}$, thus indicating a wide span of concentrations in RBH that emphasize the point-source nature of Cu within RBH.

Similar to the current study, a high correlation between magnetic susceptibility and metals at harbour terminals was observed in Hong Kong Harbour (Chan et al., 2001; Yim et al., 2004), which was related to general shipping contamination. However, the strong Cr component, as found in RBH, was not determined in these studies.

5.5. Microplastics

The occurrence of microplastics is closely related to the magnitude of anthropogenic activity (population density and proximity; Bellasi et al., 2020). Bellasi et al. (2020) attribute common input sources for lakes and rivers to tributaries, on-water activities, tourism or improper dumping. In our study, the dependence on public areas is clearly reflected in the given PET concentration and distribution of handpicked plastic pieces (Fig. 11).

5.6. Bioindicators

Although no bioindication was mentioned in their study, Wepener and Degger (2020) showed an uptake of heavy metals in mussels from the open water column (buoys at RBH entrance channel) and thus demonstrated bioavailability of contaminants in RBH. It also indicates that Cr and Cu, although loaded as particulate matter that is believed to sink rapidly to the bottom, is in suspension long enough to be taken up by filter feeders. However, lower vulnerability was observed in ostracods in similar metal contaminated environments (Millward et al., 2004). It is reported that high metal concentrations in marine environments lead to increase in malformation rates in foraminifera, but these can also be triggered by strong salinity variation or oxygen deficiency (e. g. Frontalini and Coccioni, 2008; Geslin et al., 2000; Stouff et al., 1999). Based on our observations and in accordance with Yanko et al. (1998), increased metal concentrations reduced the abundance and diversity of calcareous microfauna and diatom flora in RBH.

The prevalence of metal contaminants in RBH is clearly observable and as a primary response, the autochthonous diatom community is composed of species that are adapted to tolerate critical to very heavy levels of pollution. In the current sample set, teratological forms do not occur to any significant level. This may be due timing between sampling and the most recent pollution event, with diatom community turnover already having been initiated. On a secondary level, diatom composition is responding to osmotic pressure variability brought about by environmental pressures (Taylor et al., 2007), such as salinity, and tidal currents. In summary, we strongly encourage a more detailed systematic study to elaborate the effective bioavailability to organisms including invertebrates and vertebrates. This does not only allow the development of a more detailed bioindication system, but also allows to evaluate a warning level of sea food collected in the harbour by local residents.

6. Conclusions

RBH is strongly impacted by anthropogenic activities. Sources of metals and plastic in sediment are clearly identified. Hydrodynamic processes, influenced by wind, tides, and vessel propeller wash, affect microplastic accumulation, sediment distribution, and associated elemental concentrations. Microplastic pollution is recognizable throughout publicly accessible parts of RBH (i.e. PET).

The zonation of RBH via endmember modelling defines distinct sub-basins. Cu and Cr show very high concentrations in SB-II – the main operational basin with dry and breakbulk berths for import and export. Consequently, the bulk terminals (SB-II a-c; with increased Cr, Cu, Cd and Ni concentrations) and Small Craft Harbour (Cr, Cu) were identified as metal point sources. The metal pollution results in high malformation rates in foraminifera, and high proportions of ostracods within the calcareous microfauna at stations with highest metal concentrations. Diatoms are adversely affected by the high levels of contaminants in the harbour basin, to the extent of zones of low productivity and occurrences.

Cr and Cu concentrations in surface sediments from 2012 and 2018, as well as short sediment cores (recovered in 2018) mirror the pollution history, with increasing Cr concentrations towards the present time, preceded by a spike of Cu. Additionally, through correlating Cr concentrations and magnetic susceptibility, multiple cores reflect on spatial and historical metal pollution. This enables to quantify the load of metal (Cr) polluted sediment to an estimated volume of almost 2 million m^3 .

The maximum Cr concentration measured in 2018 in RBH is about three times higher than the concentration recently reported for international ports. Consequently, metal contamination in RBH poses a potential environmental threat to the adjacent marine ecosystem by sediment resuspension and remobilization of accumulated metals, and by the dredging related transfer of contaminated dredged sediment to open water placement sites. However, it remains to be confirmed if metals such as Cr are present in the sediment in a bioavailable form

considering chromium ore and ferrochrome particles probably account for the high concentrations of this metal in sediment in RBH.

CRedit authorship contribution statement

Paul Mehlhorn: Conceptualization, Investigation, Formal analysis, Writing – original draft, Writing – review & editing. **Finn Viehberg:** Conceptualization, Validation, Writing – original draft, Writing – review & editing, Funding acquisition. **Kelly Kirsten:** Investigation, Writing – original draft. **Brent Newman:** Investigation, Formal analysis, Writing – original draft, Writing – review & editing, Funding acquisition. **Peter Frenzel:** Investigation, Writing – original draft, Funding acquisition. **Olga Gildeeva:** Investigation, Writing – original draft. **Andrew Green:** Investigation, Visualization, Writing – original draft. **Annette Hahn:** Investigation, Writing – original draft. **Torsten Haberzettl:** Conceptualization, Writing – original draft, Supervision, Funding acquisition, Writing – review & editing, Project administration.

Declaration of competing interest

The authors declare that they have no known competing financial interests or personal relationships that could have appeared to influence the work reported in this paper.

Acknowledgements

This work was supported by the German Federal Ministry of Education and Research [grant numbers: 03F0798A, 03F0798B, 03F0798C] and is part of project TRACES (Tracing Human and Climate impact in South Africa) within the SPACES II Program (Science Partnerships for the Assessment of Complex Earth System Processes). The field work support by George Best is gratefully acknowledged. We acknowledge Anchor Energy (Pty) Ltd. for permission to use the multibeam data set. Doug Slogrove and Gaynor Deacon are acknowledged in this regard. We thank Transnet National Ports Authority for permission to use metal concentration data for the 2012 survey. The 2012 survey was funded by Transnet National Ports Authority and the CSIR through project Definition of baseline metal concentration models for assessing metal contamination of sediment from South African coastal waters (grant number: SIMS4401). We also thank Antonia Schell for semi-quantitative distribution data of plastic particles and Dirk Merten (both Friedrich-Schiller-University Jena) for ICP-MS and -OES analyses. Tammo Meyer (University of Greifswald) shared knowledge and equipment for aqua regia digestion. The cores were scanned with the ITRAX (CS-8) of GEOPOLAR at the University of Bremen. Klaus Jost kindly contributed the historical image of Richards Bay Harbour during the construction phase. Mike Steinich and Sebastian Lorenz (University of Greifswald) are acknowledged for their integral involvement in data collection.

References

- Bate, G.C., Smailes, P.A., Adams, J.B., 2004. Benthic Diatoms in the Rivers and Estuaries of South Africa Water Research Commission report, 1107.
- Begg, G., 1978. The estuaries of Natal: a resource inventory report to the Natal Town and Regional Planning Commission conducted under the auspices of the Oceanographic Research Institute, Durban. In: Natal Town and Regional Planning Report, 41, pp. 1–657.
- Belando, M.D., Marín, A., Aboal, M., García-Fernández, A.J., Marín-Guirao, L., 2017. Combined in situ effects of metals and nutrients on marine biofilms: shifts in the diatom assemblage structure and biological traits. *Sci. Total Environ.* 574, 381–389. <https://doi.org/10.1016/j.scitotenv.2016.08.197>.
- Bellasi, A., Binda, G., Pozzi, A., Galafassi, S., Volta, P., Bettinetti, R., 2020. Microplastic contamination in freshwater environments: a review, focusing on interactions with sediments and benthic organisms. *Environments* 7 (4), 30. <https://doi.org/10.3390/environments7040030>.
- Benson, R.H., Maddocks, R.F., 1964. In: *Recent Ostracods of Knysna Estuary, Cape Province, Union of South Africa*, 5. The University of Kansas Paleontological Contributions, pp. 1–39.
- Birch, G.F., Lee, J.-H., Tanner, E., Fortune, J., Munksgaard, N., Whitehead, J., Coughanowr, C., Agius, J., Chrispijn, J., Taylor, U., Wells, F., Bellas, J., Besada, V., Viñas, L., Soares-Gomes, A., Cordeiro, R.C., Machado, W., Santelli, R.E., Vaughan, M., Cameron, M., Brooks, P., Crowe, T., Ponti, M., Airoidi, L., Guerra, R., Puente, A., Gómez, A.G., Zhou, G.J., Leung, K.M.Y., Steinberg, P., 2020. Sediment metal enrichment and ecological risk assessment of ten ports and estuaries in the world harbours project. *Mar. Pollut. Bull.* 155, 111129. <https://doi.org/10.1016/j.marpolbul.2020.111129>.
- Blott, S.J., Pye, K., 2001. GRADISTAT: a grain size distribution and statistics package for the analysis of unconsolidated sediments. *Earth Surf. Process. Landforms* 26 (11), 1237–1248. <https://doi.org/10.1002/esp.261>.
- Cattaneo, A., Couillard, Y., Wunsam, S., Courcelles, M., 2004. Diatom taxonomic and morphological changes as indicators of metal pollution and recovery in Lac Dufault (Québec, Canada). *J. Paleolimnol.* 32 (2), 163–175. <https://doi.org/10.1023/B:JOPL.0000029430.78278.a5>.
- Chan, L., Ng, S., Davis, A., Yim, W., Yeung, C., 2001. Magnetic properties and heavy-metal contents of contaminated seabed sediments of Penny Bay, Hong Kong. *Mar. Pollut. Bull.* 42 (7), 569–583. [https://doi.org/10.1016/S0025-326X\(00\)00203-4](https://doi.org/10.1016/S0025-326X(00)00203-4).
- Cloete, C.E., 1979. The transfer of pollutants in two southern hemispheric oceanic systems. In: *Proceedings of a Workshop Held at Plettenberg Bay, South Africa, 23–26 April 1975*. South African Scientific Programmes Report No. 39.
- Cloete, C.E., Oliff, W.D., 1976. *South African Marine Pollution Survey Report 1974–1975*. National Scientific Programmes Unit: CSIR.
- Corcoran, P.L., 2015. Benthic plastic debris in marine and fresh water environments. *Environ. Sci. Process. Impacts* 17 (8), 1363–1369. <https://doi.org/10.1039/C5EM00188A>.
- Dearing, J., 1994. *Environmental Magnetic Susceptibility. Using the Bartington MS2 System*. Chi Publ, Kenilworth.
- Department of Environmental Affairs, 2012a. *2nd South Africa Environment Outlook. A Report on the State of the Environment. Executive Summary*. Department of environmental Affairs, Pretoria, 60 pp.
- Department of Environmental Affairs, 2012b. In: *National Environmental Management: Integrated Coastal Management Act, 2008 (Act No. 24 of 2008)*. National Action List for the Screening of Dredged Material Proposed for Marine Disposal in Term of Section 73 of the National Environmental Management: Integrated Coastal Management Act, 2008 (Act No. 24 of 2008). *Government Gazette (35602)*, pp. 6–9.
- Dietze, E., Dietze, M., 2019. Grain-size distribution unmixing using the R package EMMAgeo. *E&G Quat. Sci. J.* 68 (1), 29–46. <https://doi.org/10.5194/egqsj-68-29-2019>.
- Dietze, E., Maussion, F., Ahlborn, M., Diekmann, B., Hartmann, K., Henkel, K., Kasper, T., Lockot, G., Opitz, S., Haberzettl, T., 2014. Sediment transport processes across the tibetan plateau inferred from robust grain-size end members in lake sediments. *Clim. Past* 10 (1), 91–106. <https://doi.org/10.5194/cp-10-91-2014>.
- Dingle, R.V., 1992. Quaternary ostracods from the continental margin off South-Western Africa. Part I. Dominant taxa. *Ann. S. Afr. Mus.* 102, 1–89.
- Dingle, R.V., 1993. Quaternary ostracods from the continental margin off South-Western Africa. Part II. Minor taxa. *Ann. S. Afr. Mus.* 103, 1–165.
- Ellwood, B.B., Brett, C.E., MacDonald, W.D., 2007. Magnetostratigraphy susceptibility of the upper ordovician kope formation, northern Kentucky. *Palaeogeogr. Palaeoclimatol. Palaeoecol.* 243 (1–2), 42–54. <https://doi.org/10.1016/j.palaeo.2006.07.003>.
- Fath, A., 2019. *Mikroplastik*. Springer, Berlin Heidelberg.
- Fatoki, O.S., Mathabatha, S., 2004. An assessment of heavy metal pollution in the East London and Port Elizabeth harbours. *WSA* 27 (2). <https://doi.org/10.4314/wsa.v27i2.4997>.
- Folk, R.L., Ward, W.C., 1957. Brazos River bar [Texas]; a study in the significance of grain size parameters. *J. Sediment. Res.* 27 (1), 3–26. <https://doi.org/10.1306/74D70646-2B21-11D7-8648000102C1865D>.
- Förstner, U., Wittmann, G.T.W., 1981. *Metal Pollution in the Aquatic Environment*. Springer, Berlin Heidelberg.
- Frontalini, F., Coccioni, R., 2008. Benthic foraminifera for heavy metal pollution monitoring: a case study from the Central Adriatic Sea coast of Italy. *Estuar. Coast. Shelf Sci.* 76 (2), 404–417. <https://doi.org/10.1016/j.ecss.2007.07.024>.
- Fürstenberg, S., Gründler, N., Meschner, S., Frenzel, P., 2017. Microfossils in surface sediments of brackish waters on the west coast of South Africa and their palaeoecological implications. *Afr. J. Aquat. Sci.* 42 (4), 329–339. <https://doi.org/10.2989/16085914.2017.1406326>.
- Geslin, E., Stouff, V., Debenay, J.-P., Lesourd, M., 2000. Environmental variation and foraminiferal test abnormalities. In: Landman, N.H., Jones, D.S., Martin, R.E. (Eds.), *Environmental Micropaleontology*, 15. Springer US, Boston, MA, pp. 191–215.
- Goodenough, C.K., 2003. *The Local Global Nexus: A Case Study of Richards Bay*.
- Greenfield, R., Wepener, V., Degger, N., Brink, K., 2011. Richards Bay harbour: metal exposure monitoring over the last 34 years. *Mar. Pollut. Bull.* 62 (8), 1926–1931. <https://doi.org/10.1016/j.marpolbul.2011.04.026>.
- Haberzettl, T., 2015. Advances in limnogeology and paleolimnology: with a special focus on corroborated chronologies using paleomagnetic secular variations. *Jena, Univ., Habil.-Schr.*, 2015. Friedrich-Schiller-Universität Jena. <http://nbn-resolving.de/urn:nbn:de:gbv:27-20160107-133023-6>.
- Haberzettl, T., Fey, M., Lücke, A., Maidana, N.I., Mayr, C., Ohlendorf, C., Schäbitz, F., Schleser, G.H., Wille, M., Zolitschka, B., 2005. Climatically induced lake level changes during the last two millennia as reflected in sediments of Laguna Potrok Aike, southern Patagonia (Santa Cruz, Argentina). *J. Paleolimnol.* 33 (3), 283–302. <https://doi.org/10.1007/s10933-004-5331-z>.
- Haberzettl, T., Anselmetti, F.S., Bowen, S.W., Fey, M., Mayr, C., Zolitschka, B., Ariztegui, D., Mauz, B., Ohlendorf, C., Kastner, S., Lücke, A., Schäbitz, F., Wille, M., 2009. Late pleistocene dust deposition in the patagonian steppe - extending and refining the paleoenvironmental and tephrochronological record from Laguna

- protok aike back to 55ka. *Quat. Sci. Rev.* 28 (25–26), 2927–2939. <https://doi.org/10.1016/j.quascirev.2009.07.021>.
- Haberzettl, T., St-Onge, G., Lajeunesse, P., 2010. Multi-proxy records of environmental changes in Hudson Bay and strait since the final outburst flood of Lake Agassiz-Ojibway. *Mar. Geol.* 271 (1–2), 93–105. <https://doi.org/10.1016/j.margeo.2010.01.014>.
- Haberzettl, T., Kirsten, K.L., Kasper, T., Franz, S., Reinwarth, B., Baade, J., Daut, G., Meadows, M.E., Su, Y., Mäusbacher, R., 2019. Using ²¹⁰Pb-data and paleomagnetic secular variations to date anthropogenic impact on a lake system in the Western Cape, South Africa. *Quat. Geochronol.* 51, 53–63. <https://doi.org/10.1016/j.quageo.2018.12.004>.
- Hahn, A., Gerdts, G., Völker, C., Niebühr, V., 2019. Using FTIRS as pre-screening method for detection of microplastic in bulk sediment samples. *Sci. Total Environ.* 689, 341–346. <https://doi.org/10.1016/j.scitotenv.2019.06.227>.
- Hanson, P.J., Evans, D.W., Colby, D.R., Zdanowicz, V.S., 1993. Assessment of elemental contamination in estuarine and coastal environments based on geochemical and statistical modeling of sediments. *Mar. Environ. Res.* 36, 237–266. [https://doi.org/10.1016/0141-1136\(93\)90091-D](https://doi.org/10.1016/0141-1136(93)90091-D).
- Hatfield, R.G., Stoner, J.S., Carlson, A.E., Reyes, A.V., Housen, B.A., 2013. Source as a controlling factor on the quality and interpretation of sediment magnetic records from the northern North Atlantic. *Earth Planet. Sci. Lett.* 368, 69–77. <https://doi.org/10.1016/j.epsl.2013.03.001>.
- Kasper, T., Haberzettl, T., Doberschütz, S., Daut, G., Wang, J., Zhu, L., Nowaczyk, N., Mäusbacher, R., 2012. Indian Ocean summer monsoon (IOSM)-dynamics within the past 4 ka recorded in the sediments of Lake Nam Co, central Tibetan Plateau (China). *Quat. Sci. Rev.* 39, 73–85. <https://doi.org/10.1016/j.quascirev.2012.02.011>.
- Kerste, M., Smedes, F., 2002. Normalization procedures for sediment contaminants in spatial and temporal trend monitoring. *J. Environ. Monit.* 4, 109–115. <https://doi.org/10.1039/b108102k>.
- Kirsten, K.L., Fell, J., Frenzel, P., Meschner, S., Kasper, T., Wüdsch, M., Meadows, M.E., Haberzettl, T., 2018. The spatial heterogeneity of micro- and meio-organisms and their significance in understanding coastal system dynamics. *Estuar. Coast. Shelf Sci.* 213, 98–107. <https://doi.org/10.1016/j.ecss.2018.08.011>.
- Lisé-Pronovost, A., St-Onge, G., Gogorza, C., Haberzettl, T., Preda, M., Kliem, P., Francus, P., Zolitschka, B., 2013. High-resolution paleomagnetic secular variations and relative paleointensity since the Late Pleistocene in southern North America. *Quat. Sci. Rev.* 71, 91–108. <https://doi.org/10.1016/j.quascirev.2012.05.012>.
- Long, E.R., Macdonald, D.D., Smith, S.L., Calder, F.D., 1995. Incidence of adverse biological effects within ranges of chemical concentrations in marine and estuarine sediments. *Environ. Manag.* 19, 81–97. <https://doi.org/10.1007/BF02472006>.
- Long, E.R., Ingersoll, C.G., Macdonald, D.D., 2006. Calculation and uses of mean sediment quality guideline quotients: a critical review. *Environ. Sci. Technol.* 40, 1726–1736. <https://doi.org/10.1021/es058012d>.
- Marshall, J.S., Mellinger, D.L., 1980. An in situ experimental method for toxicological studies on natural plankton communities. In: Eaton, J.G., Parrish, P.R., Hendricks, A. C. (Eds.), *Aquatic Toxicology*. ASTM International, 100 Barr Harbor Drive, PO Box C700, West Conshohocken, PA 19428-2959, pp. 27–39.
- Millward, R.N., Carman, K.R., Fleeger, J.W., Gambrell, R.P., Portier, R., 2004. Mixtures of metals and hydrocarbons elicit complex responses by a benthic invertebrate community. *J. Exp. Mar. Biol. Ecol.* 310 (1), 115–130. <https://doi.org/10.1016/j.jembe.2004.04.004>.
- Nayar, K.G., Sharqawy, M.H., Banchik, L.D., Lienhard, V., J.H., 2016. Thermophysical properties of seawater: a review and new correlations that include pressure dependence. *Desalination* 390, 1–24. <https://doi.org/10.1016/j.desal.2016.02.024>.
- Newman, B.K., Watling, R.J., 2007. Definition of baseline metal concentrations for assessing metal enrichment of sediment from the south-eastern cape Coastline of South Africa. *Water SA* 33. <https://doi.org/10.4314/wsa.v33i5.184089>.
- Nguyen-Deroche, T.L.N., Caruso, A., Le, T.T., Bui, T.V., Schoefs, B., Tremblin, G., Morant-Manceau, A., 2012. Zinc affects differently growth, photosynthesis, antioxidant enzyme activities and phytochelatin synthase expression of four marine diatoms. *Sci. World J.* 2012, 982957. <https://doi.org/10.1100/2012/982957>.
- Ohlendorf, C., Fey, M., Massafiero, J., Haberzettl, T., Laprida, C., Lücke, A., Maidana, N. I., Mayr, C., Oehlerich, M., Ramon Mercuau, J., Wille, M., Corbella, H., St-Onge, G., Schabitz, F., Zolitschka, B., 2014. Late Holocene hydrology inferred from lacustrine sediments of Laguna Cháitel (southeastern Argentina). *Palaeogeogr. Palaeoclimatol. Palaeoecol.* 411, 229–248. <https://doi.org/10.1016/j.palaeo.2014.06.030>.
- Oliff, W.D., Turner, W.D., 1976. In: *National Marine Pollution Surveys, East Coast Section: 2nd Annual Report*. NIWR, Durban, p. 172.
- Parent, B., Barras, C., Jorissen, F., 2018. An optimised method to concentrate living (Rose Bengal-stained) benthic foraminifera from sandy sediments by high density liquids. *Mar. Micropaleontol.* 144, 1–13. <https://doi.org/10.1016/j.marmicro.2018.07.003>.
- Sah, D., Verma, P.K., Kandikonda, M.K., Lakhani, A., 2019. Chemical fractionation, bioavailability, and health risks of heavy metals in fine particulate matter at a site in the Indo-Gangetic Plain, India. *Environ. Sci. Pollut. Res. Int.* 26 (19), 19749–19762. <https://doi.org/10.1007/s11356-019-05144-8>.
- Schell, A.C., 2019. Makrofauna, Schalenchemie und Sedimentkomponenten als Indikatoren Anthropogener Einflüsse im Hafengebiet von Richards Bay. Südafrika, Jena.
- Schoonees, J.S., Theron, A.K., Bevis, D., 2006. Shoreline accretion and sand transport at groynes inside the port of Richards Bay. *Coast. Eng.* 53 (12), 1045–1058. <https://doi.org/10.1016/j.coastaleng.2006.06.006>.
- Schwab, R., Becker, W. (Eds.), 2014. 1983/84, 1st ed. Springer Berlin, Berlin.
- Semensatto, D.L., Dias-Brito, D., 2007. Alternative saline solutions to float foraminiferal tests. *J. Foraminifer. Res.* 37 (3), 265–269. <https://doi.org/10.2113/gsjfr.37.3.265>.
- Shannon, C.E., 1948. A mathematical theory of communication. *Bell Syst. Tech. J.* 27 (3), 379–423. <https://doi.org/10.1002/j.1538-7305.1948.tb01338.x>.
- Sharqawy, M.H., Lienhard, J.H., Zubair, S.M., 2010. Thermophysical properties of seawater: a review of existing correlations and data. *Desalin. Water Treat.* 16 (1–3), 354–380. <https://doi.org/10.5004/dwt.2010.1079>.
- Stouff, V., Geslin, E., Debenay, J.-P., Lesourd, M., 1999. Origin of morphological abnormalities in ammonia (Foraminifera) studies in laboratory and natural environments. *J. Foraminifer. Res.* 29 (2), 152–170. <https://doi.org/10.2113/gsjfr.29.2.152>.
- Strobel, P., Kasper, T., Frenzel, P., Schitteck, K., Quick, L.J., Meadows, M.E., Mäusbacher, R., Haberzettl, T., 2019. Late quaternary palaeoenvironmental change in the year-round rainfall zone of South Africa derived from peat sediments from vankervelsvlei. *Quat. Sci. Rev.* 218, 200–214. <https://doi.org/10.1016/j.quascirev.2019.06.014>.
- Taylor, J.C., Harding, W.R., Archibald, C.G.M., 2007. *An Illustrated Guide to Some Common Diatom Species From South Africa*. Water Research Commission, Gezina, South Africa, 11 pp.
- Vermeulen, L.A., Wepener, V., 1999. Spatial and temporal variations of metals in Richards Bay Harbour (RBH), South Africa. *Mar. Pollut. Bull.* 39 (1–12), 304–307. [https://doi.org/10.1016/S0025-326X\(99\)00083-1](https://doi.org/10.1016/S0025-326X(99)00083-1).
- Wepener, V., Degger, N., 2020. Monitoring metals in South African harbours between 2008 and 2009, using resident mussels as indicator organisms. *Afr. Zool.* 1–11. <https://doi.org/10.1080/15627020.2020.1799720>.
- Wepener, V., Vermeulen, L.A., 2005. A note on the concentrations and bioavailability of selected metals in sediments of Richards Bay Harbour, South Africa. *Water SA* 31 (4), 589–596. <https://doi.org/10.4314/wsa.v31i4.5149>.
- Whitfield, A.K., 1992. A characterization of southern african estuarine systems. *South. Afr. J. Aquat. Sci.* 18 (1–2), 89–103. <https://doi.org/10.1080/10183469.1992.9631327>.
- Williams, G.E., Steenkamp, J.D., 2006. Heavy mineral processing at Richards bay minerals. *South. Afr. Pyrometall.* 2006, 181–188.
- Wüdsch, M., Haberzettl, T., Kirsten, K.L., Kasper, T., Zabel, M., Dietze, E., Baade, J., Daut, G., Meschner, S., Meadows, M.E., Mäusbacher, R., 2016. Sea level and climate change at the southern Cape coast, South Africa, during the past 4.2 kyr. *Palaeogeogr. Palaeoclimatol. Palaeoecol.* 446, 295–307. <https://doi.org/10.1016/j.palaeo.2016.01.027>.
- Yanko, V., Muna, A., Kaminski, M., 1998. Morphological deformities of benthic foraminiferal tests in response to pollution by heavy metals; implications for pollution monitoring. *J. Foraminifer. Res.* 28 (3), 177–200.
- Yim, W.-S., Huang, G., Chan, L.S., 2004. Magnetic susceptibility study of late quaternary inner continental shelf sediments in the Hong Kong SAR, China. *Quat. Int.* 117 (1), 41–54. [https://doi.org/10.1016/S1040-6182\(03\)00115-0](https://doi.org/10.1016/S1040-6182(03)00115-0).